| L Number | Hits | Search Text | DB | Time stamp |
|---|---|---|---|---|
| 12 | 2 | improve adj AOA | USPAT; US-PGPUB; EPO; JPO; DERWENT; IBM_TDB | 2003/10/09 10:48 |
| 13 | 4 | (improve adj accuracy) with AOA | USPAT; US-PGPUB; EPO; JPO; DERWENT; IBM_TDB | 2003/10/09 10:33 |
| 16 | 12 | improve with accuracy with AOA | USPAT; US-PGPUB; EPO; JPO; DERWENT; IBM_TDB | 2003/10/09 10:29 |
| 17 | 2 | (increase adj accuracy) with AOA | USPAT; US-PGPUB; EPO; JPO; DERWENT; IBM_TDB | 2003/10/09 10:31 |
| 18 | 9 | (increase with accuracy) with AOA | USPAT; US-PGPUB; EPO; JPO; DERWENT; IBM_TDB | 2003/10/09 10:31 |
| 19 | 1 | improve adj DOA | USPAT; US-PGPUB; EPO; JPO; DERWENT; IBM_TDB | 2003/10/09 10:33 |
| 20 | 1 | (improve adj accuracy) with DOA | USPAT; US-PGPUB; EPO; JPO; DERWENT; IBM_TDB | 2003/10/09 10:34 |
| 21 | 10 | (improve with accuracy) with DOA | USPAT; US-PGPUB; EPO; JPO; DERWENT; IBM_TDB | 2003/10/09 10:34 |
| 22 | 0 | E911 with AOA | USPAT; US-PGPUB; EPO; JPO; DERWENT; IBM_TDB | 2003/10/09 10:48 |
| 24 | 0 | (E911 FCC) with (angle adj arrival) | USPAT; US-PGPUB; EPO; JPO; DERWENT; IBM_TDB | 2003/10/09 10:54 |
| 23 | 2 | FCC with AOA | USPAT; US-PGPUB; EPO; JPO; DERWENT; IBM_TDB | 2003/10/09 10:53 |
| 25 | 10 | (E911 FCC) same ((angle adj arrival) AOA) | USPAT; US-PGPUB; EPO; JPO; DERWENT; IBM_TDB | 2003/10/09 10:57 |

| L Number | Hits | Search Text | DB | Time stamp |
|---|---|---|---|---|
| 26 | 2 | (E911 FCC) same ((direction adj arrival) DOA) | USPAT; US-PGPUB; EPO; JPO; DERWENT; IBM_TDB | 2003/10/09 10:58 |
| 27 | 28 | emergency same ((angle adj arrival) AOA) | USPAT; US-PGPUB; EPO; JPO; DERWENT; IBM_TDB | 2003/10/09 10:58 |
| 28 | 10 | emergency same ((direction adj arrival) DOA) | USPAT; US-PGPUB; EPO; JPO; DERWENT; IBM_TDB | 2003/10/09 10:58 |
| 30 | 218 | (AOA DOA (angle adj arrival) (direction adj arrival) DOA).ti. | USPAT; US-PGPUB; EPO; JPO; DERWENT; IBM_TDB | 2003/10/09 11:39 |
| 31 | 0 | (E911 FCC) and ((AOA DOA (angle adj arrival) (direction adj arrival) DOA).ti.) | USPAT; US-PGPUB; EPO; JPO; DERWENT; IBM_TDB | 2003/10/09 11:21 |
| 32 | 4 | emergency and ((AOA DOA (angle adj arrival) (direction adj arrival) DOA).ti.) | USPAT; US-PGPUB; EPO; JPO; DERWENT; IBM_TDB | 2003/10/09 11:21 |
| 33 | 631 | 455/456.1.ccls. | USPAT; US-PGPUB; EPO; JPO; DERWENT; IBM_TDB | 2003/10/09 11:38 |
| 34 | 60 | (AOA DOA (angle adj arrival) (direction adj arrival) DOA) and 455/456.1.ccls. | USPAT; US-PGPUB; EPO; JPO; DERWENT; IBM_TDB | 2003/10/09 11:39 |
| 35 | 9 | ((AOA DOA (angle adj arrival) (direction adj arrival) DOA) and 455/456.1.ccls.) and (phase with amplitude) | USPAT; US-PGPUB; EPO; JPO; DERWENT; IBM_TDB | 2003/10/09 11:41 |
| 36 | 1 | (((AOA DOA (angle adj arrival) (direction adj arrival) DOA) and 455/456.1.ccls.) and (phase same amplitude)) not (((AOA DOA (angle adj arrival) (direction adj arrival) DOA) and 455/456.1.ccls.) and (phase with amplitude)) | USPAT; US-PGPUB; EPO; JPO; DERWENT; IBM_TDB | 2003/10/09 11:42 |

## Advanced Search: INSPEC - 1969 to date (INZZ)

limit

Search history:

| No. | Database | Search term | Info added since | Results | |
|---|---|---|---|---|---|
| 1 | INZZ | strongest ADJ multipath | unrestricted | 7 | show titles |
| 2 | INZZ | strongest ADJ component AND multipath | unrestricted | 1 | show titles |

hide | delete all searches...

Enter your search term(s): Search tips

whole document

Information added since: or: none
(YYYYMMDD)

search

Select special search terms from the following list(s):

- Classification codes A: Physics, 0-1
- Classification codes A: Physics, 2-3
- Classification codes A: Physics, 4-5
- Classification codes A: Physics, 6
- Classification codes A: Physics, 7
- Classification codes A: Physics, 8
- Classification codes A: Physics, 9
- Classification codes B: Electrical & Electronics, 0-5
- Classification codes B: Electrical & Electronics, 6-9
- Classification codes C: Computer & Control, 0-9
- Classification codes D: Information Technology, 0-9
- Treatment codes
- INSPEC sub-file
- Publication types
- Language of publication

## Document

Select the documents you wish to save or order by clicking the box next to the document, or click the link above the document to order directly.

save order locally as: PDF document include search strategy

☐ **document 1 of 1** Order Document

**INSPEC - 1969 to date (INZZ)**

**Accession number & update**
6309731, B1999-09-6250F-139, C1999-09-7410F-042; 19990801.

**Title**
Spread spectrum in mobile communications. 3. Computer simulations.

**Author(s)**
Stular-M; Tomazic-S.

**Author affiliation**
Fakulteta za Elektrotehniko, Ljubljana Univ, Slovenia.

**Source**
Elektrotehniski-Vestnik (Slovenia), vol.66, no.3, p.222-8, 1999. , Published: Electrotech. Soc. Slovenia.

**CODEN**
ELVEA2.

**ISSN**
ISSN: 0013-5852.

**Availability**
SICI: 0013-5852(1999)66:3L.222:SSMC; 1-E.

**Publication year**
1999.

**Language**
EN.

**Publication type**
J Journal Paper.

**Treatment codes**
P Practical; T Theoretical or Mathematical.

**Abstract**
In order to deepen our knowledge and understanding of spread spectrum principles, computer simulations of a direct sequence spread spectrum (DSSS) and narrow-band system (NB) were carried out. An experimental base-band DSSS system is considered. It consists of a transmitter, mobile propagation channel and receiver. In the transmitter, coding and spreading of the data signal take place. The main part of the mobile propagation channel is a FIR filter. Besides this, noise and jamming signals are added to the desired signal in the channel. In the receiver, the received signal is correlated with the locally generated PN signal and decoded afterwards. As regards decoding, there are several alternatives available. Namely, the DSSS principle allows us to resolve components which are mutually delayed (usually as a result of time-dispersive effects of

**multipath** propagation) for at least chip time T/sub c/. We can therefore form a decision variable by combining more than one received **component.** A decoding algorithm on the basis of the **strongest component** is shown. (4 refs).

**Descriptors**

digital-simulation; FIR-filters; mobile-radio; spread-spectrum-communication; telecommunication-computing.

**Keywords**

direct sequence spread spectrum; narrow band system; mobile propagation channel; FIR filter; jamming signals; time dispersive effects; **multipath** propagation; decision variable; decoding algorithm.

**Classification codes**

B6250F (Mobile radio systems).
C7410F (Communications computing).

**Copyright statement**

Copyright 1999, IEE.

SEARCH RESULTS [PDF Full-Text (460 KB)] PREVIOUS NEXT DOWNLOAD CITATION

# Direction finding/polarization estimation-dipole and/or loop triad(s)

Wong, K.T.
Dept. of Electron. Eng., Chinese Univ. of Hong Kong, Shatin;

*This paper appears in:* **Aerospace and Electronic Systems, IEEE Transactions on**
On page(s): 679-684
Volume: 37, Issue: 2, Apr 2001
ISSN: 0018-9251
References Cited: 21
CODEN: IEARAX
INSPEC Accession Number: 7001876

**Abstract:**
This paper shows (1) how measurement of the three Cartesian components of the electrical-field or magnetic-field suffices for multisource azimuth/elevation direction finding and polarization estimation, and (2) how the vector cross-product direction-of-arrival estimator is fully applicable even when the dipole triad is arbitrarily displaced from the loop triad

**Index Terms:**
direction-of-arrival estimation electromagnetic wave polarisation radio direction-finding Cartesian components dipole triad direction-of-arrival estimator loop triad multisource azimuth/elevation direction finding polarization estimation vector cross-product

**Documents that cite this document**
Select link to view other documents in the database that cite this one.

SEARCH RESULTS [PDF Full-Text (460 KB)] PREVIOUS NEXT DOWNLOAD CITATION

# Direction Finding/Polarization Estimation—Dipole and/or Loop Triad(s)

KAINAM THOMAS WONG, Senior Member, IEEE
Chinese University of Hong Kong

**This paper shows 1) how measurement of the three Cartesian components of the electrical-field *or* magnetic-field suffices for multisource azimuth/elevation direction finding and polarization estimation, and 2) how the vector cross-product direction-of-arrival estimator is fully applicable even when the dipole triad is arbitrarily displaced from the loop triad.**

Manuscript received June 1, 2000; revised October 24, 2000; released for publication December 21, 2000.

IEEE Log No. T-AES/37/2/06339.

Refereeing of this contribution was handled by Dr. Jim P. Y. Lee.

Part of this work was presented at the 1999 *IEEE International Conference on Circuits & Systems.*

This research work was supported by Direct Grants 2050187 and 1050247 and Mainline Grant 44M5010, all from Hong Kong's Research Grant Council.

Author's address: Department of Electronic Engineering, Chinese University of Hong Kong, Shatin, NT, Hong Kong, E-mail: (ktwong@ieee.org).



## I. INTRODUCTION

A series of recent papers, [3–12, 14–18, 20, 21] among others, investigates the use of collocated six-component electromagnetic vector sensors for diversely polarized direction-of-arrival (DOA) estimation. A collocated six-component vector sensor consists of three identical and collocated but orthogonally oriented electrically short dipoles (called a dipole triad) plus three identical collocated but orthogonally oriented magnetically small loops (called a loop triad). All six component-antennas are spatially collocated in a point-like geometry. The collocated six-component vector sensor offers the following advantages: 1) the polarization diversity among the vector sensor's component antennas allows that incident sources to be separated on account of their polarization differences in addition to their azimuth/elevation angular differences; 2) the spatial collocation of all component antennas in the vector sensor means no *spatial* phase delay in the vector sensor steering vector; hence, near-field sources may be located by an individual vector sensor as well as far-field sources; and 3) in a multisource scenario, each source's three Cartesian direction cosine estimates (and thus each source's azimuth angle estimate and the elevation angle estimate) are automatically paired without further post-processing. Theoretical performance bounds for direction finding using the collocated six-component vector sensors have been defined and derived in [3, 5].

A variety of eigenstructure-based direction finding, polarization estimation and tracking schemes [6–12, 14–18, 20, 21] have deployed these collocated six-component vector sensors in diverse array configurations for various signal scenarios using the vector cross-product DOA estimator. This vector cross-product DOA estimator exploits all six Cartesian components of the incident electromagnetic field to estimate the $k$th source's amplitude-normalized Poynting vector $\mathbf{p}_k$, which, in turn, gives estimates of the source's elevation angle $\theta_k$ (measured from the positive $z$-axis) and the azimuth angle $\phi_k$ (measured from the positive $x$-axis):

$$\mathbf{p}_k \stackrel{\text{def}}{=} \begin{bmatrix} p_{x_k} \\ p_{y_k} \\ p_{z_k} \end{bmatrix} = \frac{\mathbf{e}_k \times \mathbf{h}_k^*}{\|\mathbf{e}_k\| \quad \|\mathbf{h}_k^*\|} \stackrel{\text{def}}{=} \begin{bmatrix} u_k \\ v_k \\ w_k \end{bmatrix} = \begin{bmatrix} \sin\theta_k & \cos\phi_k \\ \sin\theta_k & \sin\phi_k \\ \cos\theta_k & \end{bmatrix} \tag{1}$$

where $*$ denotes complex conjugation, $\mathbf{e}_k$ and $\mathbf{h}_k$, respectively, denote the $k$th source's electric-field vector and magnetic-field vector, $u_k$, $v_k$, and $w_k$, respectively, represent the $k$th source's direction-cosines along the $x$-axis, the $y$-axis, and the $z$-axis. This vector cross-product DOA estimation approach complements the customary interferometry direction finding approach, which estimates the

spatial phase delay among the data sets collected at physically displaced antennas.

The six-component electromagnetic vector-sensor, however, suffers from mutual coupling between its dipole triad and its loop triad. If only one triad (but not both) is deployed or if some significant distance separates the two triads, then the above mentioned coupling problem may be mitigated. Moreover deploying only one triad reduces antenna and receiver electronic hardware costs, simplifies algorithmic complexity, completely avoids the inter-dipole/loop triad mutual coupling problem, and eliminates the need to synchronize the phase between the dipole triad and the loop triad.

This work shows 1) how a *dipole* triad by itself suffices for multisource azimuth/elevation direction finding and polarization estimation, 2) how a *loop* triad by itself suffices for multisource azimuth/elevation direction finding and polarization estimation, and 3) how the vector cross-product DOA estimator remains fully applicable for a pair of dipole triad and loop triad spatially displaced by an arbitrary and (possibly) unknown distance (rather than being collocated). The above contrasts with the case of a collocated pair of perpendicularly oriented dipoles (commonly used in mobile communications), which is insufficient for exact estimation of the sources' arrival angles. In [19], however, it is shown that two horizontally oriented and magnetically small loops (plus an optional vertically oriented short dipole) can *approximately* estimate the sources' azimuth angles. Such an antenna array set-up matches the polarization of the wireless handset transmitter's strong vertical electric-field and can be used to retrofit dumb antenna-array receivers at the cellular base-station for downlink transmission beamforming.

## II. MATHEMATICAL MODELS OF STEERING VECTORS

The $k$th unit-power completely polarized[1] transverse electromagnetic wave, having traveled through a homogeneous isotropic medium, is characterized by the electric-field vector $\mathbf{e}_k$ and the magnetic-field vector $\mathbf{h}_k$, expressible in Cartesian coordinates as [3, 4]:

$$\begin{bmatrix}\mathbf{e}_k\\ \mathbf{h}_k\end{bmatrix} \stackrel{\text{def}}{=} \begin{bmatrix} e_x(\theta_k,\phi_k,\gamma_k,\eta_k)\\ e_y(\theta_k,\phi_k,\gamma_k,\eta_k)\\ e_z(\theta_k,\gamma_k,\eta_k)\\ h_x(\theta_k,\phi_k,\gamma_k,\eta_k)\\ h_y(\theta_k,\phi_k,\gamma_k,\eta_k)\\ h_z(\theta_k,\gamma_k)\end{bmatrix}$$

$$\stackrel{\text{def}}{=} \underbrace{\begin{bmatrix} \cos\phi_k\cos\theta_k & -\sin\phi_k\\ \sin\phi_k\cos\theta_k & \cos\phi_k\\ -\sin\theta_k & 0\\ -\sin\phi_k & -\cos\phi_k\cos\theta_k\\ \cos\phi_k & -\sin\phi_k\cos\theta_k\\ 0 & \sin\theta_k\end{bmatrix}}_{\stackrel{\text{def}}{=}\Theta(\theta_k,\phi_k)} \underbrace{\begin{bmatrix}\sin\gamma_k e^{j\eta_k}\\ \cos\gamma_k\end{bmatrix}}_{\stackrel{\text{def}}{=}\mathbf{g}_k} \tag{2}$$

where $0 \le \theta_k < \pi/2$ denotes the signal's elevation angle measured from the vertical $z$-axis, $0 \le \phi_k < 2\pi$ symbolizes the azimuth angle measured from the positive $x$-axis, $0 \le \gamma_k < \pi/2$ refers to the auxiliary polarization angle, and $-\pi \le \eta_k < \pi$ represents the polarization phase difference. Note that $\Theta(\theta_k,\phi_k)$ depends only on the angular parameters, whereas $\mathbf{g}_k$ depends only on the polarizational parameters. Also, $\|\mathbf{e}_k\| = \|\mathbf{h}_k\| = 1$ for all values of $(\theta_k,\phi_k,\gamma_k,\eta_k)$.

The dipole triad has the steering vector $\mathbf{a}_k = \mathbf{e}_k$. The loop triad has the steering vector $\mathbf{a}_k = \mathbf{h}_k$. A dipole triad plus a displaced but identically oriented loop triad (with the loop triad located at $(d_x,d_y,d_z)$ relative to the dipole triad) has the steering vector

$$\mathbf{a}_k = \begin{bmatrix}\mathbf{e}_k\\ \mathbf{h}_k q_H(u_k,v_k)\end{bmatrix},$$

where $q_H(u_k,v_k)$ is defined as $e^{j2\pi(d_x u_k + d_y v_k + d_z w_k)/\lambda}$ and represents the *spatial* phase-factor relating the measurement at the loop triad to that at the dipole triad. $\lambda$ denotes the signals' wavelength. For reference,

$$\mathbf{a}_k = \begin{bmatrix}\mathbf{e}_k\\ \mathbf{h}_k\end{bmatrix}$$

for the collocated six-component vector sensor.

The dipole triad, the loop triad, or the dipole-triad-plus-loop-triad displaced pair may be used as a multicomponent element in a multielement array for direction finding and polarization estimation, just as the collocated six-component vector sensor has been used in [3–12, 14–18, 20, 21]. Specifically, in [8] a single collocated six-component vector sensor (along with a *temporal-invariance* version of ESPRIT[2]) to estimate the arrival angles and polarization states of multiple pure tones, while in [10, 21] the same is done for multiple frequency-hop (FH) signals. In [6, 7, 17, 18] a number of collocated six-component vector sensors are employed in a sparse (thinned) $L \times M$ rectangular array without incurring any cyclic ambiguity in the final estimates of the sources' Cartesian direction cosines by the use of a *spatial-invariance* version of ESPRIT. In

[1] Partially polarized or unpolarized sources may be handled using the techniques presented in [12].

[2] ESPRIT [2] is a closed-form eigenstructure-based parameter estimation technique that requires the data to possess certain "invariance" structures.

[9, 20], arbitrarily and irregularly spaced three-dimensional arrays of collocated six-component vector sensors are proposed in conjunction with a MUSIC[3]-based algorithm that needs no initial coarse estimates to start off MUSIC's iterative search. In [11, 16], it is shown how the above arbitrarily spaced collocated six-component vector sensors are handled, using a *polarization-invariance* version of ESPRIT, when their locations are unknown. In all above mentioned schemes, the collocated six-component vector sensor may be substituted by the dipole triad, or the loop triad, or the dipole-triad-plus-loop-triad displaced pair; and this paper shows how. Without reciting the algorithmic details, all aforementioned schemes involve eigenstructure-based parameter estimation algorithmic steps that lead to an estimate of each incident source's steering vector, correct to within an *unknown* complex-value scalar $c_k$. That is, available somewhere in each algorithm is the estimate $\hat{\mathbf{a}}_k \approx c_k \mathbf{a}_k$. (The approximation becomes a straight equality in noiseless or asymptotic cases.) The question is whether $\hat{\mathbf{a}}_k$ suffices to unambiguously estimate the $k$th source's arrival angles and polarization states when $\mathbf{a}_k$ corresponds to the steering vector of a dipole triad, a loop triad, or a dipole-triad-plus-loop-triad displaced pair. The answer is "yes" and the following section shows how.

## III. ESTIMATION FORMULAS FOR THE ARRIVAL ANGLES AND POLARIZATION PARAMETERS

The key observation is that $\|\mathbf{e}_k\| = \|\mathbf{h}_k\| = \|\mathbf{p}_k\| = 1$ for all $(\theta_k, \phi_k, \gamma_k, \eta_k)$. This means that the uncertainty in $\hat{\mathbf{a}}_k$ due to $|c_k|$ may be removed by amplitude-normalizing $\hat{\mathbf{a}}_k$ in the cases of the dipole triad and the loop triad to produce a unity Frobenius norm. Algebraic and trigonometric manipulations on this normalized $\hat{\mathbf{a}}_k/\|\hat{\mathbf{a}}_k\|$ then produce five real-valued nonlinear equations, leading to unambiguous estimation of $\{\theta_k, \phi_k, \gamma_k, \eta_k\}$.

### A. For Dipole Triad

If dipole triads are deployed, $\hat{\mathbf{a}}_k = c_k \mathbf{e}_k$ under noiseless or asymptotic conditions. Hence,

$$\frac{\hat{\mathbf{a}}_k e^{-j\angle[\hat{\mathbf{a}}_k]_3}}{\|\hat{\mathbf{a}}_k\|} = \begin{bmatrix} -\cos\theta_k \cos\phi_k \sin\gamma_k + \cos\gamma_k \sin\phi_k \cos\eta_k \\ -\cos\theta_k \sin\phi_k \sin\gamma_k - \cos\gamma_k \cos\phi_k \cos\eta_k \\ \sin\theta_k \sin\gamma_k \end{bmatrix} + j \begin{bmatrix} -\cos\gamma_k \sin\phi_k \sin\eta_k \\ \cos\gamma_k \cos\phi_k \sin\eta_k \\ 0 \end{bmatrix} \tag{3}$$

where $[\cdot]_i$ refers to the $i$th element in the bracketed vector and $\angle$ denotes the angle of the ensuing entity.

[3]MUSIC [1] is an iterative eigenstructure-based parameter estimation technique.

The above array manifold model has not accounted for the dipoles' mutual coupling effects; however, good isolation and balance among the dipoles can minimize intratriad mutual coupling and renders the above array manifold model a very realistic approximation The above expression shows that the real and imaginary parts of $e^{-j\angle[\hat{\mathbf{a}}_k]_3}\hat{\mathbf{a}}_k/\|\hat{\mathbf{a}}_k\|$, as five real-valued separate entities, producing for each incident source five separate nonlinear real-valued equations relating the four unknown signal parameters $\{\theta_k, \phi_k, \gamma_k, \eta_k\}$. Manipulation of these equations gives

$$\hat{\phi}_k = \begin{cases} \tan^{-1}\dfrac{-\mathrm{Im}\{[\hat{\mathbf{a}}_k e^{-j\angle[\hat{\mathbf{a}}_k]_3}]_1\}}{\mathrm{Im}\{[\hat{\mathbf{a}}_k e^{-j\angle[\hat{\mathbf{a}}_k]_3}]_2\}}, & \text{if } \mathrm{Im}\{[\hat{\mathbf{a}}_k e^{-j\angle[\hat{\mathbf{a}}_k]_3}]_1\} < 0 \\ \tan^{-1}\dfrac{-\mathrm{Im}\{[\hat{\mathbf{a}}_k e^{-j\angle[\hat{\mathbf{a}}_k]_3}]_1\}}{\mathrm{Im}\{[\hat{\mathbf{a}}_k e^{-j\angle[\hat{\mathbf{a}}_k]_3}]_2\}} + \pi, & \text{if } \mathrm{Im}\{[\hat{\mathbf{a}}_k e^{-j\angle[\hat{\mathbf{a}}_k]_3}]_1\} \geq 0 \end{cases} \tag{4}$$

$$\hat{\theta}_k = \tan^{-1}\left\{\left\|\frac{[\hat{\mathbf{a}}_k]_3}{\mathrm{Re}\{[\hat{\mathbf{a}}_k]_1 e^{-j\angle[\hat{\mathbf{a}}_k]_3}\}\cos\hat{\phi}_k + \mathrm{Re}\{[\hat{\mathbf{a}}_k]_2 e^{-j\angle[\hat{\mathbf{a}}_k]_3}\}\sin\hat{\phi}_k}\right\|\right\} \tag{5}$$

$$\hat{\gamma}_k = \sin^{-1}\left\{\frac{\|[\hat{\mathbf{a}}_k]_3\|}{\sin\hat{\theta}_k}\right\} \tag{6}$$

$$\hat{\eta}_k = [\hat{\mathbf{a}}_k e^{-j\angle[\hat{\mathbf{a}}_k]_3}]_1 \sin\hat{\phi}_k + [\hat{\mathbf{a}}_k e^{-j\angle[\hat{\mathbf{a}}_k]_3}]_2 \cos\hat{\phi}_k. \tag{7}$$

Thus, the unknown complex-valued scalar ambiguity $c_k$ in $\hat{\mathbf{a}}_k$ needs to cause no ambiguity in the estimation of the arrival angles and polarization parameters.

### B. For Loop Triad

If loop triads are deployed, $\hat{\mathbf{a}}_k = c_k \mathbf{h}_k$ under noiseless or asymptotic conditions. Hence,

$$\frac{\hat{\mathbf{a}}_k e^{-j\angle[\hat{\mathbf{a}}_k]_3}}{\|\hat{\mathbf{a}}_k\|} = \begin{bmatrix} -\cos\theta_k \cos\phi_k \cos\gamma_k + \sin\gamma_k \sin\phi_k \cos\eta_k \\ -\cos\theta_k \sin\phi_k \cos\gamma_k - \sin\gamma_k \cos\phi_k \cos\eta_k \\ \sin\theta_k \cos\gamma_k \end{bmatrix} + j \begin{bmatrix} -\sin\gamma_k \sin\phi_k \sin\eta_k \\ \sin\gamma_k \cos\phi_k \sin\eta_k \\ 0 \end{bmatrix}. \tag{8}$$

The above array manifold model has not accounted for the loops' mutual coupling effects; however, good isolation and balance among the loops can minimize intratriad mutual coupling and renders the above array manifold model a very realistic approximation. The $z$-axis component of $\mathbf{h}_k$ is always real in value regardless of the values of $(\theta, \phi, \gamma, \eta)$. With the left-hand-side of (8) already available, (8) produces for each incident source five nonlinear real-valued equations relating the four unknown

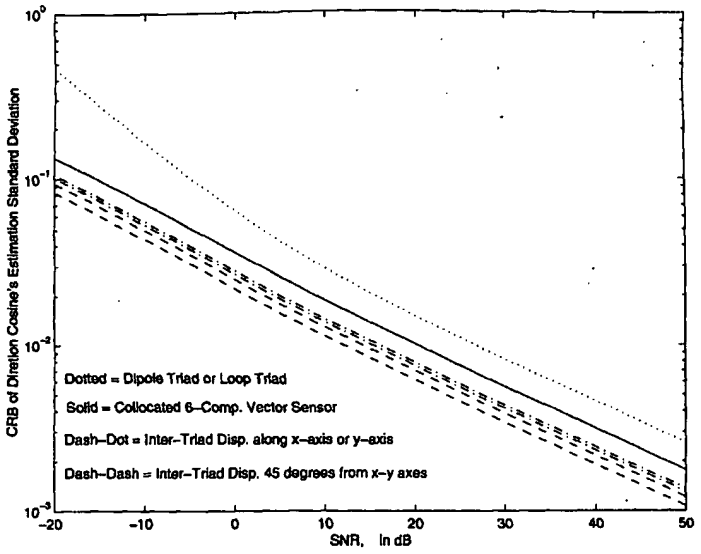


Fig. 1. CRBs for various multicomponent antennas versus SNR. There are two incident narrowband completely polarized uncorrelated sources with $(u_1, v_1, \eta_1, \gamma_1) = (0.41, 0.31, \pi/2, \pi/4)$ and $(u_2, v_2, \eta_2, \gamma_2) = (0.59, 0.49, -\pi/2, \pi/4)$. 200 snapshots used at each SNR value.

signal parameters. Manipulation of these equations gives

$$\hat{\phi}_k = \begin{cases} \tan^{-1}\dfrac{-\mathrm{Im}[\hat{\mathbf{a}}_k e^{-j\angle[\hat{\mathbf{a}}_k]_3}]_1}{\mathrm{Im}[\hat{\mathbf{a}}_k e^{-j\angle[\hat{\mathbf{a}}_k]_3}]_2}, & \text{if } \mathrm{Im}[\hat{\mathbf{a}}_k e^{-j\angle[\hat{\mathbf{a}}_k]_3}]_1 < 0 \\ \tan^{-1}\dfrac{-\mathrm{Im}[\hat{\mathbf{a}}_k e^{-j\angle[\hat{\mathbf{a}}_k]_3}]_1}{\mathrm{Im}[\hat{\mathbf{a}}_k e^{-j\angle[\hat{\mathbf{a}}_k]_3}]_2} + \pi, & \text{if } \mathrm{Im}[\hat{\mathbf{a}}_k e^{-j\angle[\hat{\mathbf{a}}_k]_3}]_1 \geq 0 \end{cases} \tag{9}$$

$$\hat{\theta}_k = \tan^{-1}\left\{\left\|\frac{\mathrm{Re}\{[\hat{\mathbf{a}}_k e^{-j\angle[\hat{\mathbf{a}}_k]_3}]_3\}}{\mathrm{Re}\{[\hat{\mathbf{a}}_k e^{-j\angle[\hat{\mathbf{a}}_k]_3}]_1\}\cos\hat{\phi}_k + \mathrm{Re}\{[\hat{\mathbf{a}}_k e^{-j\angle[\hat{\mathbf{a}}_k]_3}]_2\}\sin\hat{\phi}_k}\right\|\right\} \tag{10}$$

$$\hat{\gamma}_k = \cos^{-1}\left\{\frac{\mathrm{Re}\{[\hat{\mathbf{a}}_k]_3\}}{\sin\hat{\theta}_k}\right\} \tag{11}$$

$$\hat{\eta}_k = \angle\{[\hat{\mathbf{a}}_k e^{-j\angle[\hat{\mathbf{a}}_k]_3}]_1 + \cos\hat{\phi}\cos\hat{\theta}_k\cos\hat{\gamma}_k + [\hat{\mathbf{a}}_k e^{-j\angle[\hat{\mathbf{a}}_k]_3}]_2 + \sin\hat{\phi}_k\cos\hat{\theta}_k\cos\hat{\gamma}_k\}. \tag{12}$$

## C. For Displaced Dipole-Triad-Plus-Loop-Triad Pair

Recalling that

$$\hat{\mathbf{a}}_k = c_k\begin{bmatrix}\mathbf{e}_k \\ q_H(u_k, v_k)\mathbf{h}_k\end{bmatrix}$$

under noiseless or asymptotic conditions and that $\|q_H(u_k, v_k)\| = 1$,

$$\frac{(c_k\hat{\mathbf{e}}_k)\times(c_k q_H(u_k,v_k)\hat{\mathbf{h}}_k)^*}{\|(c_k\hat{\mathbf{e}}_k)\times(c_k q_H(u_k,v_k)\hat{\mathbf{h}}_k)^*\|} = \underbrace{q_H(u_k, v_k)\mathbf{p}_k}_{\stackrel{\text{def}}{=}\tilde{\mathbf{p}}_k} \tag{13}$$

where $\times$ denotes the vector cross product. Hence,

$$\mathbf{p}_k = \tilde{\mathbf{p}}_k e^{-j\angle[\tilde{\mathbf{p}}_k]_3} = \begin{bmatrix}u_k \\ v_k \\ w_k\end{bmatrix} = \begin{bmatrix}\sin\theta_k\cos\phi_k \\ \sin\theta_k\sin\phi_k \\ \cos\theta_k\end{bmatrix} \tag{14}$$

with

$$\tilde{\mathbf{p}}_k = \frac{[\mathbf{I}_3 \vdots \mathbf{0}_3]\hat{\mathbf{a}}_k \times [\mathbf{0}_3 \vdots \mathbf{I}_3]\hat{\mathbf{a}}_k}{\|[\mathbf{I}_3 \vdots \mathbf{0}_3]\hat{\mathbf{a}}_k \times [\mathbf{0}_3 \vdots \mathbf{I}_3]\hat{\mathbf{a}}_k\|} \tag{15}$$

where $\mathbf{I}_3$ symbolizes a $3\times 3$ identity matrix, and $\mathbf{0}_3$ refers to a $3\times 3$ zero matrix. Hence,

$$\hat{\theta}_k = \arcsin(\sqrt{[\hat{\mathbf{p}}_k]_1^2 + [\hat{\mathbf{p}}_k]_2^2}) = \arccos([\hat{\mathbf{p}}_k]_3) \tag{16}$$

$$\hat{\phi}_k = \arctan([\hat{\mathbf{p}}_k]_2/[\hat{\mathbf{p}}_k]_1) \tag{17}$$

$$\hat{\gamma}_k = \arctan\frac{[\hat{\mathbf{g}}_k]_1}{[\hat{\mathbf{g}}_k]_2} \tag{18}$$

$$\hat{\eta}_k = \angle[\hat{\mathbf{g}}_k]_1 - \angle[\hat{\mathbf{g}}_k]_2 \tag{19}$$

where

$$\hat{\mathbf{g}}_k \stackrel{\text{def}}{=} [\tilde{\Theta}_k^H\tilde{\Theta}_k]^{-1}\tilde{\Theta}_k^H\hat{\mathbf{a}}_k \tag{20}$$

$$\tilde{\Theta}_k \stackrel{\text{def}}{=} [\mathbf{I}_3 \vdots q_H(\sin\hat{\theta}_k\cos\hat{\phi}_k, \sin\hat{\theta}_k\sin\hat{\phi}_k)\mathbf{I}_3]\Theta(\hat{\theta}_k, \hat{\phi}_k). \tag{21}$$

## IV. COMPARATIVE CRAMER–RAO BOUND PERFORMANCE

Fig. 1 plots the Cramer–Rao bound (CRB) [3] versus the signal-to-noise ratio (SNR) for the

several multicomponent antenna types discussed in this work under a scenario involving two closely spaced, completely polarized, narrowband, uncorrelated far-field sources under additive white Gaussian noise. The source parameters are with $(u_1,v_1,\eta_1,\gamma_1) = (0.41,0.31,\pi/2,\pi/4)$ and $(u_2,v_2,\eta_2,\gamma_2) = (0.59,0.49,-\pi/2,\pi/4)$. There are 200 snapshots used at each SNR value.

The dipole triad and the loop triad has an exactly identical CRB curve, which is 3 dB higher than that of the collocated six-component vector sensor. This is expected because the former has half the number of component-antennas as the latter. The dash-dot and dash curves all refer to the dipole-triad-plus-loop-triad displaced pair case, revealing the effects of the intertriad displacement axis' length and orientation. The two dash-dot curves and the top dash curve all correspond to an half-wavelength intertriad axis, whereas the bottom dash curve refers to a five-wavelength intertriad axis. The top dash-dot curve has the intertriad displacement aligned along the $x$-axis; the lower dash-dot has the intertriad displacement aligned along the $y$-axis; and the upper dash curve has the inter-triad displacement 45° from the $x$-$y$ axes. It may be observed that a longer intertriad axis gives better estimates because of the larger geometric aperture that results. The axis orientation that optimizes estimation performance is the orientation onto which the incident sources project the farthest angular separation. In the present signal scenario, the 45° orientation (clockwise from the positive $x$-axis) gives the two sources a wider angular separation than when the intertriad axis is aligned either along the $x$-axis or along the $y$-axis.

## REFERENCES


[1] Schmidt, R. O. (1986)
Multiple emitter location and signal parameter estimation.
*IEEE Transactions on Antennas and Propagation*, **34**, 3 (Mar. 1986), 276–280.

[2] Roy, R., and Kailath, T. (1989)
ESPRIT-estimation of signal parameters via rotational invariance techniques.
*IEEE Transactions on Acoustics, Speech, Signal Processing*, **37**, 7 (July 1989), 984–995.

[3] Nehorai, A., and Paldi, E.(1991)
Vector-sensor array processing for electromagnetic source localization.
*IEEE Transactions on Signal Processing*, **42**, 2 (Feb. 1994), 376–398; and in *Asilomar Conference*, 1991, 566–572.

[4] Li, J. (1993)
Direction and polarization estimation using arrays with small loops and short dipoles.
*IEEE Transactions on Antennas and Propagation*, **41**, 3 (Mar. 1993), 379–387.

[5] Hochwald, B., and Nehorai, A. (1995)
Polarimetric modeling and parameter estimation with applications to remote sensing.
*IEEE Transactions on Signal Processing*, **43**, 8 (Aug. 1995), 1923–1935.

[6] Wong, K. T., and Zoltowski, M. D. (1996)
High accuracy 2D angle estimation with extended aperture vector sensor array.
In *Proceedings of International Conference on Acoustics, Speech, Signal Processing*, **5** (1996), 2789–2792.

[7] Zoltowski, M. D., and Wong, K. T. (1997)
Polarization diversity and extended-aperture spatial diversity to mitigate fading-channel effects with a sparse array of electric dipoles or magnetic loops.
In *Proceedings of IEEE International Vehicular Technology Conference*, 1997, 1163–1167.

[8] Wong, K. T., and Zoltowski, M. D. (1997)
Uni-Vector-Sensor ESPRIT for multi-source azimuth, elevation, and polarization estimation.
*IEEE Transactions on Antennas and Propagation*, **45**, 10 (Oct. 1997), 1467–1474.

[9] Wong, K. T., and Zoltowski, M. D. (1997)
Self-initiating MUSIC-based direction finding in polarization beamspace.
*IEE Radar'97 Conference*, IEE Publication 449, 328–333.

[10] Wong, K. T. (1998)
Adaptive geolocation and blind beamforming for wideband fast frequency-hop signals of unknown hop sequences and unknown arrival angles using an electromagnetic vector-sensor.
In *Proceedings of IEEE International Conference on Communications*, **2** (1998), 758–762.

[11] Wong, K. T., and Zoltowski, M. D. (1998)
Closed-form direction-finding with arbitrarily spaced electromagnetic vector-sensors at unknown locations.
In *Proceedings of IEEE International Conference on Acoustics, Speech and Signal Processing*, **4** (1998), 1949–1952.

[12] Wong, K. T. (1999)
Geolocation for partially polarized electromagnetic sources using multiple sparsely and uniformly spaced spatially stretched vector sensors.
In *Proceedings of IEEE International Conference on Circuits and Systems*, **3** (1999), 170–174.

[13] Wong, K. T. (1999)
A novel closed-form azimuth/elevation angle and polarization estimation technique using only electric dipole triads or only magnetic loop triads with arbitrary unknown spacings.
In *Proceedings of IEEE International Conference on Circuits and Systems*, **3** (1999), 207–210.

[14] Ho, K.-C., Tan, K.-C., and Nehorai, A. (1999)
Estimating directions of arrival of completely and incompletely polarized signals with electromagnetic vector sensors.
*IEEE Transactions on Signal Processing*, **47**, 10 (Oct. 1999), 2845–2852.

[15] Nehorai, A., and Tichavsky, P. (1999)
Cross-product algorithms for source tracking using an EM vector sensor.
*IEEE Transactions on Signal Processing*, **47**, 10 (Oct. 1999), 2863–2867.

[16] Wong, K. T., and Zoltowski, M. D. (2000)
Closed-form direction-finding and polarization estimation with arbitrarily spaced electromagnetic vector-sensors at unknown locations.
*IEEE Transactions on Antennas and Propagation*, **48**, 5 (May 2000), 671–681.

[17] Zoltowski, M. D., and Wong, K. T. (2000)
ESPRIT-based 2-D direction finding with a sparse uniform array of electromagnetic vector-sensors.
*IEEE Transactions on Signal Processing*, **48**, 8 (Aug. 2000), 2195–2204.

[18] Zoltowski, M. D., and Wong, K. T. (2000)
Closed-form eigenstructure-based direction finding using arbitrary but identical subarrays on a sparse uniform Cartesian array grid.
*IEEE Transactions on Signal Processing*, **48**, 8 (Aug. 2000), 2205–2210.

[19] Wong, K. T., and Lai, A. (2000)
Inexpensive upgrade of antenna-switching cellular base-station receivers for uplink/downlink beamforming using a magnetic-loop pair or a loop/dipole triad.
Presented at the *2000 IEEE Global Telecommunications Conference*, 1370–1374.

[20] Wong, K. T., and Zoltowski, M. D. (2000)
Self-initiating MUSIC-based direction finding & polarization estimation in spatio-polarizational beamspace.
*IEEE Transactions on Antennas and Propagation*, **48**, 9 (Sept. 2000), 1235–1245.

[21] Wong, K. T. (2001)
Geolocation/Beamforming for multiple FFH with unknown hop-sequences.
*IEEE Transactions on Aerospace and Electronic Systems*, **37**, 1 (Jan. 2001).

**Kainam Thomas (Tom) Wong** (S'85—M'97—SM'01) earned the B.S.E. (Chem. E.) from U.C.L.A. in 1985, the B.S.E.E. from the University of Colorado, Boulder, in 1987, the M.S.E.E. from the Michigan State University, East Lansing, in 1990, and the Ph.D. in E.E. from Purdue University, West Lafayette, IN in 1996.

Dr. Wong was a Manufacturing Engineer at General Motors Technical Center (Warren, MI) from 1990 to 1991, a Senior Professional Staff Member at The Johns Hopkins University Applied Physics Laboratory (Laurel, MD) from 1996 to 1998, and an Assistant Professor at Singapore's Nanyang Technological University in 1998. He has been an Assistant Professor in the Department of Electronic Engineering at the Chinese University of Hong Kong since 1998. His current interests are signal processing for communications and sensor array signal processing.

Dr. Wong is a contributing author of about 70 articles for the telecommunications section of the inaugural edition (2001) of the CRC Dictionary of Pure and Applied Physics. He serves on the Technical Program Committees of the 1999 and 2000 IEEE Wireless Communications and Networking Conference (WCNC'99, WCNC'00), the 2000 Spring IEEE Vehicular Technology Conference (VTC'00 Spring) and other conferences. He also serves on the Organizing Committees of the 2000 IEEE International Symposium on Circuits and Systems (ISCAS'00) and the Symposium 2000 on Adaptive Signal Processing, Communications and Control (AS-SPCC).

# Extended-aperture spatial diversity and polarizational diversity using a sparse array of electric dipoles or magnetic loops

Zoltowski, M.D. Wong, K.T.
Sch. of Electr. & Comput. Eng., Purdue Univ., West Lafayette, IN;

*This paper appears in:* **Vehicular Technology Conference, 1997 IEEE 47th**
05/04/1997 -05/07/1997, 4-7 May 1997
Location: Phoenix, AZ , USA
On page(s): 1163-1167 vol.2
Volume: 2, 4-7 May 1997
References Cited: 8
Number of Pages: 3 vol. xxx+2247
INSPEC Accession Number: 5773394

**Abstract:**
A novel eigenstructure scheme of extended-aperture spatial diversity and polarizational diversity is proposed for 2D arrival angle estimation. This innovational method involves uniformly spaced triads (or pairs) of electric dipoles or magnetic loops, spaced much farther apart than a half-wavelength. An ESPRIT-based step produces arrival angle estimates that suffer cyclic ambiguity due to the extended spacing. Then, a closed-form integer search is performed over a MUSIC null spectrum for all finite number of possible direction cosines in the cyclic ambiguity using the aforementioned cyclically ambiguous estimates. This approach produces highly accurate, yet unambiguous, azimuth and elevation angle estimates. This novel method facilitates (1) multipath de-correlation (independent fading), (2) coherent summation of multipaths from the same source, and (3) down-link beamforming from the base-station to the mobile

**Index Terms:**
array signal processing correlation methods direction-of-arrival estimation diversity reception eigenstructure assignment electromagnetic wave polarisation fading land mobile radio loop antennas multipath channels radio links 2D arrival angle estimation ESPRIT-based step MUSIC null spectrum azimuth estimates base-station closed-form integer search coherent summation cyclic ambiguity direction cosines down-link beamforming eigenstructure scheme electric dipoles elevation angle estimates extended-aperture polarizational diversity extended-aperture spatial diversity independent fading magnetic loops multipath decorrelation sparse array uniformly spaced triads

# Extended-Aperture Spatial Diversity & Polarizational Diversity Using a Sparse Array of Electric Dipoles or Magnetic Loops[†]

Michael D. Zoltowski
*mikedz@ecn.purdue.edu, 317-494-3512, 317-494-0880 (fax)*
*Purdue Univ., Sch. of Electrical and Computer Engineering,*
*W. Lafayette, IN 47907-1285 U.S.A.*

Kainam T. Wong
*wongkt1@jhuapl.edu, 301-953-5000 x8147, 301-953-6567 (fax)*
*Johns Hopkins University Applied Physics Lab.,*
*Laurel, MD 20723-6099 U.S.A.*

## ABSTRACT

A novel eigenstructure scheme of extended-aperture spatial diversity and polarizational diversity is herein proposed for 2D arrival angle estimation. This innovational method involves uniformly spaced triads (or pairs) of electric dipoles or magnetic loops, spaced much farther apart than a half-wavelength. An ESPRIT-based step produces arrival angle estimates that suffer cyclic ambiguity due to the extended spacing. Then, a closed-form integer search is performed over a MUSIC null spectrum for all finite number of possible direction cosines in the cyclic ambiguity, using the aforementioned cyclically ambiguous estimates. This approach produces highly accurate, yet unambiguous, azimuth and elevation angle estimates. This novel method facilitates (1) multipath de-correlation (independent fading), (2) coherent summation of multipaths from the same source, and (3) down-link beamforming from the base-station to the mobile.

## 1. INTRODUCTION

Spatial diversity and polarizational diversity improve wireless link performance. Spatial diversity and polarizational diversity are premised on the expectation that if one channel is in a deep fade, the multipaths may be constructive interfering in another channel. Note that field measurements [1] performed in a typical urban cellular environment have indicated that the horizontal and vertical polarizations have nearly equal power and are effectively uncorrelated.

In frequency-selective slow-fading environments (slow-fading implies constant fading characteristics over a short observation period), spatial diversity and polarizational diversity also allow various time-delayed multipaths to be resolved based on their distinct polarizational states as well as their spatial arrival angles. These resolved multipaths may then be constructively summed to maximize the signal-to-noise ratio. Moreover, estimates of these sources' up-link arrival angles facilitate down-link beamforming from the base-station to the mobile. Spatial diversity is realized by deploying multiple spatially displaced antennas, typically at the base station. Polarization diversity also allows signals impinging from the same direction to be resolved on the basis of their different polarizational states. As the most significant scatterers are typically close to the mobile, the base station antenna array aperture needs to extend at least over ten wavelengths to attain independent fading.

The most straightforward way to realize a larger array aperture is to use more antennas, but at increased hardware and software costs. If it is desired to estimate the impinging signals' arrival angles (for down-link beamforming and/or multipath constructive summation in frequency-selective fading as explained above) using the highly popular close-form computationally efficient eigenstructure method of ESPRIT (Estimation of Signal Parameters via Rotational Invariance Techniques) [4], then spacing adjacent array elements non-uniformly over half a wavelength would generally violate ESPRIT's requirement of two identical but translated subarrays. Uniform inter-element spacing exceeding half a wavelength, on the other hand, would lead to a set of ambiguous direction-cosine estimates. That is, the one-to-one correspondence between ESPRIT's eigenvalues and the direction-cosines would no longer exist when the uniform inter-element spacing exceeds half a wavelength. With no a-priori information, this ambiguity cannot be resolved using unpolarized scalar sensors.

This paper presents a direction-finding and polarization estimation scheme deploying a sparse array of either identical triads or identical pairs of electric dipoles of magnetic loops to extend uniform inter-element spacing beyond a half-wavelength while resolving the aforementioned cyclic ambiguity.

## 2. BASIC PRINCIPLES UNDERLYING NEW ALGORITHM

Three co-located but orthogonally oriented electric dipoles would measure all three electrical-field components of the incident electromagnetic field separately. Similarly, three co-located but orthogonally oriented magnetic loops would measure all three magnetic-field components separately. To illustrate the basic principles of the method, the algorithm is described employing an $L \times M$ rectangular array of identical triads or pairs of electric dipoles or magnetic loops. The inter-triad or inter-pair spacing $\Delta$ is assumed to be much greater than a half-wavelength to effect a large array aperture and correspondingly achieve highly accurate source direction estimates. One matrix-pencil is formed by considering the $(L-1) \times M$ triads or pairs on the first to the $(L-1)$-th rows as one sub-array and the $(L-1) \times M$ triads or pairs on the second to the $L$-th rows as the other sub-array. This matrix-pencil has a spatial invariance along the x-axis and can yield estimates of the direction-cosines $\{u_k = \sin\theta_k \cos\phi_k, \quad k = 1, \ldots, K\}$, where $0 \leq \theta_k < \pi/2$ is the signal's elevation angle measured from the vertical z-axis, $0 \leq \phi_k < 2\pi$ is the azimuth angle. The second matrix-pencil is formed by considering the $(M-1) \times L$ triads or pairs on the first to the $(M-1)$-th columns as one sub-array and the $(M-1) \times L$ triads or pairs on the second to the $M$-th rows as the other sub-array. This matrix-pencil has a spatial invariance along the y-axis and can yield estimates of the direction-cosines $\{v_j = \sin\theta_j \sin\phi_j, \quad j = 1, \ldots, K\}$. However, when the inter-triad or inter-pair spacing is greater than a half-wavelength there is an integer multiple of $2\pi$ ambiguity in the phase of each eigenvalue generated in the

[†]This research was supported by the Air Force Office of Scientific Research under grant no. F49620-95-1-0367, the National Science Foundation under under grant no. MIPS-9320890, and the Army Research Office's Focused Research Initiative under grant number DAAHO4-95-1-0246.

final stage of TLS-ESPRIT. This leads to ambiguous DOA estimates equi-spaced by $\lambda/\Delta$ in the interval $-1 \le u_k < 1$ (or $-1 \le v_k < 1$ as the case may be.) If one could resolve this ambiguity, the resulting DOA estimate would be highly accurate due to the large aperture. The key idea of this paper is to determine the minimum of the MUSIC null spectrum by stepping through all finite number of possible direction-cosine values, using the cyclically ambiguous estimates.

## 3. SPARSE ARRAY DATA MODEL

The propagation model is transverse electromagnetic plane-waves traveling through a non-conductive homogeneous isotropic medium. Under these conditions, the wavefront incident upon the array has an electric-field vector, e, and corresponding magnetic-field vector, h, that can be expressed in Cartesian coordinates in matrix form as: [2]

$$\begin{bmatrix} e_{x_k} \\ e_{y_k} \\ e_{z_k} \\ h_{x_k} \\ h_{y_k} \\ h_{z_k} \end{bmatrix} \stackrel{\text{def}}{=} \begin{bmatrix} sin\gamma_k\, cos\theta_k\, cos\phi_k\, e^{j\eta_k} - cos\gamma_k\, sin\phi_k \\ sin\gamma_k\, cos\theta_k\, sin\phi_k\, e^{j\eta_k} + cos\gamma_k\, cos\phi_k \\ -sin\gamma_k\, sin\theta_k\, e^{j\eta_k} \\ -cos\gamma_k\, cos\theta_k\, cos\phi_k - sin\gamma_k\, sin\phi_k\, e^{j\eta_k} \\ -cos\gamma_k\, cos\theta_k\, sin\phi_k + sin\gamma_k\, cos\phi_k\, e^{j\eta_k} \\ cos\gamma_k\, sin\theta_k \end{bmatrix} \quad (1)$$

$$= \begin{bmatrix} \cos\phi_k \cos\theta_k & -\sin\phi_k \\ \sin\phi_k \cos\theta_k & \cos\phi_k \\ -\sin\theta_k & 0 \\ -\sin\phi_k & -\cos\phi_k \cos\theta_k \\ \cos\phi_k & -\sin\phi_k \cos\theta_k \\ 0 & \sin\theta_k \end{bmatrix} \begin{bmatrix} \sin\gamma_k\, e^{j\eta_k} \\ \cos\gamma_k \end{bmatrix} \quad (2)$$

where $0 \le \gamma < \pi/2$ is the auxiliary polarization angle, $-\pi \le \eta < \pi$ is the polarization phase difference, $0 \le \theta < \pi$ is the signal's elevation angle measured from the vertical $z$-axis, $0 \le \phi < 2\pi$ is the azimuth angle, $Z_o$ is the transmission medium's intrinsic impedance.

$K$ co-channel signal sources are assumed to be in the far field and narrowband in the sense that the bandwidth is very small relative to the carrier frequency. Given a uniform rectangular array of the aforementioned identical triads or identical pairs of electric dipoles or magnetic loops, the $JLM \times 1$ snapshot vector (where $J = 3$ for an array of triads and $J = 2$ for an array of pairs) at time $t$ may be expressed as

$$\begin{aligned} \mathbf{z}(t) &= \sum_{k=1}^{K} s_k(t)\mathbf{q}_x(u_k) \otimes \mathbf{q}_y(v_k) \otimes \mathbf{a}(\theta_k, \phi_k, \gamma_k, \eta_k) + \mathbf{n}(t) \\ &= \mathbf{A}\mathbf{s}(t) + \mathbf{n}(t) \end{aligned} \quad (3)$$

where $\mathbf{A}$ is the $JLM \times K$ matrix:

$$\mathbf{A} \stackrel{\text{def}}{=} [\mathbf{q}_x(u_1) \otimes \mathbf{q}_y(v_1) \otimes \mathbf{a}(\theta_1, \phi_1, \gamma_1, \eta_1), \cdots, \mathbf{q}_x(u_K) \otimes \mathbf{q}_y(v_K) \otimes \mathbf{a}(\theta_K, \phi_K, \gamma_K, \eta_K)] \quad (4)$$

where

$$\mathbf{s}(t) \stackrel{\text{def}}{=} \begin{bmatrix} s_1(t) \\ \vdots \\ s_K(t) \end{bmatrix}; \quad \mathbf{n}(t) \stackrel{\text{def}}{=} \begin{bmatrix} \mathbf{n}_{1,1}(t) \\ \vdots \\ \mathbf{n}_{L,M}(t) \end{bmatrix}$$

$$\mathbf{q}_x(u_k) \stackrel{\text{def}}{=} \begin{bmatrix} e^{\frac{j2\pi 1\Delta_x u_k}{\lambda}} \\ \vdots \\ e^{\frac{j2\pi L\Delta_x u_k}{\lambda}} \end{bmatrix}; \quad \mathbf{q}_y(v_k) \stackrel{\text{def}}{=} \begin{bmatrix} e^{\frac{j2\pi 1\Delta_y v_k}{\lambda}} \\ \vdots \\ e^{\frac{j2\pi M\Delta_y v_k}{\lambda}} \end{bmatrix}$$

$s_k(t)$ is the complex baseband signal comprising the $k$-th signal arrival, $\mathbf{n}_{l,m}(t)$ is the $J \times 1$ additive zero-mean white noise vector at the $(l,m)$-th triad or pair, $\otimes$ is the Kronecker product, $\lambda$ is the wavelength associated with the center frequency, $\omega_c$, of the passband of the front end bandpass filter. Furthermore, $\mathbf{a}_k \stackrel{\text{def}}{=} \mathbf{a}(\theta_k, \phi_k, \gamma_k, \eta_k)$ is the $J \times 1$ steering vector for the $k$-th source sensed at each triad or pair. That is, for triads of dipoles:

$$\mathbf{a}_k = \begin{bmatrix} e_{x_k} \\ e_{y_k} \\ e_{z_k} \end{bmatrix} = \underbrace{\begin{bmatrix} \cos\phi_k \cos\theta_k & -\sin\phi_k \\ \sin\phi_k \cos\theta_k & \cos\phi_k \\ -\sin\theta_k & 0 \end{bmatrix}}_{\stackrel{\text{def}}{=}\mathbf{\Phi}_k} \underbrace{\begin{bmatrix} \sin\gamma_k\, e^{j\eta_k} \\ \cos\gamma_k \end{bmatrix}}_{\stackrel{\text{def}}{=}\mathbf{g}_k} \quad (5)$$

For triads of magnetic loops:

$$\mathbf{a}_k = \begin{bmatrix} h_{x_k} \\ h_{y_k} \\ h_{z_k} \end{bmatrix} = \underbrace{\begin{bmatrix} -\sin\phi_k & -\cos\phi_k \cos\theta_k \\ \cos\phi_k & -\sin\phi_k \cos\theta_k \\ 0 & \sin\theta_k \end{bmatrix}}_{\stackrel{\text{def}}{=}\mathbf{\Phi}_k} \underbrace{\begin{bmatrix} \sin\gamma_k\, e^{j\eta_k} \\ \cos\gamma_k \end{bmatrix}}_{\stackrel{\text{def}}{=}\mathbf{g}_k} \quad (6)$$

Furthermore, if dipole pairs or loop pairs are used instead of dipole triads or loop triads, then $\mathbf{a}_k$ becomes $2 \times 1$, with the appropriate Cartesian component deleted from (5) or (6). It would also be possible to have co-located mix of dipoles and loops. For example, a dipole oriented along the $x$-axis, another dipole along the $y$-axis plus a loop along the $y$-axis. When all six electromagnetic-field components are separately measured, then a simpler procedure alternative to the present algorithm may be used [5]. Note that in any case, $\mathbf{\Theta}_k$ depends only on the sources' spatial angular location and $\mathbf{g}_k$ depends only on the incident signals' polarization states. The maximum number of uncorrelated sources that the present algorithm can handle with such a $L \times M$ rectangular array of vector-sensors is $\min\{J(L-1)M - 1, JL(M-1) - 1\}$.

With a total of $N > K$ snapshots taken at the distinct times $\{t_n, n = 1, \ldots, N\}$, the present direction-finding problem is to determine $\{\theta_k, \phi_k,\ k = 1, \ldots, K\}$ from the $JLM \times N$ data set:

$$\mathbf{Z} \stackrel{\text{def}}{=} \begin{bmatrix} \mathbf{Z}_{1,1} \\ \vdots \\ \mathbf{Z}_{1,M} \\ \vdots \\ \vdots \\ \mathbf{Z}_{L,1} \\ \vdots \\ \mathbf{Z}_{L,M} \end{bmatrix} = \begin{bmatrix} \mathbf{z}_{1,1}(t_1) & \cdots & \mathbf{z}_{1,1}(t_N) \\ \vdots & & \vdots \\ \mathbf{z}_{1,M}(t_1) & \cdots & \mathbf{z}_{1,M}(t_N) \\ \vdots & & \vdots \\ \vdots & & \vdots \\ \mathbf{z}_{L,1}(t_1) & \cdots & \mathbf{z}_{L,1}(t_N) \\ \vdots & & \vdots \\ \mathbf{z}_{L,M}(t_1) & \cdots & \mathbf{z}_{L,M}(t_N) \end{bmatrix} \quad (7)$$

where each of the $LM$ sub-matrices $\mathbf{z}_{l,m}$ of size $J \times N$ corresponds to data measured at the $(l,m)$-th vector-sensor.

## 4. 2D ANGLE ESTIMATION WITH A SPARSE ARRAY OF ELECTRIC DIPOLES OR A SPARSE ARRAY OF MAGNETIC LOOPS

The first step in ESPRIT is to compute the $K$ ($JLM \times 1$) signal-subspace eigenvectors by eigen-decomposing the $JLM \times JLM$ data covariance matrix $\mathbf{ZZ}^T$. Although two distinct matrix-pencil pairs are to be formed, only one eigen-decomposition of this data covariance matrix is necessary because both matrix-pencils are formed from the same $JLM \times N$ data set. Let $\mathbf{E}_s$ be the $JLM \times K$ matrix composed of the $K$ eigenvectors corresponding to the $K$ largest eigenvalues of the $JLM \times JLM$ sample covariance matrix $\mathbf{R}_{zz} = \mathbf{ZZ}^H$. Due to the invariance associated with the two

subarrays along the $x$-axis, it follows from the snapshot model in (3) that $\mathbf{E}_S$ asymptotically approaches $\mathbf{E}_S = \mathbf{AT}$, where $\mathbf{T}$ is an unknown $K \times K$ non-singular matrix to be determined. $\mathbf{T}$ is necessarily non-singular because both $\mathbf{A}$ and $\mathbf{E}_S$ are full-rank matrices.

### 4.1. Deriving the low-variance but ambiguous estimates of $u_k$:

For the matrix pencil with spatial invariance along the $x$-axis, define $\mathbf{E}_1^u$ as the first $J(L-1)M$ rows of $\mathbf{E}_S$ and $\mathbf{E}_2^u$ as the last $J(L-1)M$ rows of $\mathbf{E}_S$, that is:

$$\mathbf{E}_1^u = \left[\mathbf{I}_{J(L-1)M} \;\vdots\; \mathbf{O}_{JM}\right]\mathbf{E}_S = \mathbf{A}_1^u\mathbf{T} \tag{8}$$

$$\mathbf{E}_2^u = \left[\mathbf{O}_{JM} \;\vdots\; \mathbf{I}_{J(L-1)M}\right]\mathbf{E}_S = \mathbf{A}_2^u\mathbf{T} \tag{9}$$

where $\mathbf{A}_1^u = \left[\mathbf{q}_x^{(1)}(u_1)\otimes\mathbf{q}_y(v_1)\otimes\mathbf{a}(\theta_1,\phi_1,\gamma_1,\eta_1),\cdots,\right.$
$\left.\mathbf{q}_x^{(1)}(u_K)\otimes\mathbf{q}_y(v_K)\otimes\mathbf{a}(\theta_K,\phi_K,\gamma_K,\eta_K)\right]$

$\mathbf{A}_2^u = \mathbf{A}_1^u\mathbf{\Phi}^u = \left[\mathbf{q}_x^{(2)}(u_1)\otimes\mathbf{q}_y(v_1)\otimes\mathbf{a}(\theta_1,\phi_1,\gamma_1,\eta_1),\cdots,\right.$
$\left.\mathbf{q}_x^{(2)}(u_K)\otimes\mathbf{q}_y(v_K)\otimes\mathbf{a}(\theta_K,\phi_K,\gamma_K,\eta_K)\right]$

$$\mathbf{q}_x^{(1)}(u_k) \stackrel{\text{def}}{=} \begin{bmatrix} e^{\frac{j2\pi\Delta_x 1u_k}{\lambda}} \\ \vdots \\ e^{\frac{j2\pi\Delta_x(L-1)u_k}{\lambda}} \end{bmatrix} \quad \mathbf{q}_x^{(2)}(u_k) \stackrel{\text{def}}{=} \begin{bmatrix} e^{\frac{j2\pi\Delta_x 2u_k}{\lambda}} \\ \vdots \\ e^{\frac{j2\pi\Delta_x Lu_k}{\lambda}} \end{bmatrix}$$

and $\mathbf{I}_i$ is a $i \times i$ identity matrix and $\mathbf{O}_i$ is an $i \times i$ matrix whose elements are all zeroes. In noiseless or asymptotic cases, there exists a $K \times K$ non-singular matrix $\mathbf{\Psi}^u$ relating the two $J(L-1)M \times K$ full-rank matrices $\mathbf{E}_1^u$ and $\mathbf{E}_2^u$ [4]:

$$\mathbf{E}_1^u\mathbf{\Psi}^u = \mathbf{E}_2^u \Rightarrow \quad \mathbf{A}_1^u\mathbf{T}^u\mathbf{\Psi}^u = \mathbf{A}_2^u\mathbf{T}^u \tag{10}$$

$$\Rightarrow \quad \mathbf{\Psi}^u = \{(\mathbf{E}_1^u)^H\mathbf{E}_1^u\}^{-1}\{(\mathbf{E}_1^u)^H\mathbf{E}_2^u\} \tag{11}$$

$$\Rightarrow \quad \mathbf{\Psi}^u = (\mathbf{T}^u)^{-1}\mathbf{\Phi}^u\mathbf{T}^u \tag{12}$$

where $\mathbf{\Phi}^u$ is a $K \times K$ diagonal matrix whose diagonal elements $\{[\mathbf{\Phi}^u]_{kk} = e^{j\frac{2\pi}{\lambda}\Delta_x u_k},\ k = 1,\ldots,K\}$ constitute the eigenvalues of $\mathbf{\Psi}^u$. Because $\Delta_x \gg \frac{\lambda}{2}$ and $-1 \le u_k \le 1$, there exists a set of cyclically related candidates for the estimation of $u_k$:

$$\hat{u}_k^{(n_u)} = \mu_k + n_u\frac{\lambda}{\Delta_x}, \quad \mu_k = \frac{\angle[\mathbf{\Phi}^u]_{kk}}{2\pi\Delta_x/\lambda}$$

$$\left\lceil\frac{\Delta_x}{\lambda}(-1-\mu_k)\right\rceil \le n_u \le \left\lfloor\frac{\Delta_x}{\lambda}(1-\mu_k)\right\rfloor \tag{13}$$

where $\lceil x\rceil$ is the smallest integer not less than $x$, $\lfloor x\rfloor$ is the largest integer not greater than $x$, and $\angle$ refers to the principal argument. Furthermore, the eigenvector corresponding to the eigenvalue $[\mathbf{\Phi}^u]_{kk}$ is the $k$-th column of $(\mathbf{T}^u)^{-1}$, where $\mathbf{T}^u = \mathbf{P}^u\mathbf{T}$ and $\mathbf{P}^u$ is an unknown permutation matrix. In more realistic cases where noise is present and when only a finite number of snapshots are available, all of the above estimates become only approximate.

### 4.2. Deriving the low-variance but ambiguous estimates of $v_k$:

Similarly, for the matrix pencil with spatial invariance along the $y$-axis, define $\mathbf{E}_1^v$ and $\mathbf{E}_2^v$ as:

$$\mathbf{E}_1^v = \underbrace{\begin{bmatrix} \tilde{\mathbf{I}}_1 & & \\ & \ddots & \\ & & \tilde{\mathbf{I}}_1 \end{bmatrix}}_{L\text{-block-diagonal}}\mathbf{E}_S = \mathbf{A}_1^v\mathbf{T} \tag{14}$$

$$\mathbf{E}_2^v = \underbrace{\begin{bmatrix} \tilde{\mathbf{I}}_2 & & \\ & \ddots & \\ & & \tilde{\mathbf{I}}_2 \end{bmatrix}}_{L\text{-block-diagonal}}\mathbf{E}_S = \mathbf{A}_2^v\mathbf{T} \tag{15}$$

where

$\mathbf{A}_1^v = \left[\mathbf{q}_x(u_1)\otimes\mathbf{q}_y^{(1)}(v_1)\otimes\mathbf{a}(\theta_1,\phi_1,\gamma_1,\eta_1),\cdots,\right.$
$\left.\mathbf{q}_x(u_K)\otimes\mathbf{q}_y^{(1)}(v_K)\otimes\mathbf{a}(\theta_K,\phi_K,\gamma_K,\eta_K)\right]$

$\mathbf{A}_2^v = \mathbf{A}_1^v\mathbf{\Phi}^v = \left[\mathbf{q}_x(u_1)\otimes\mathbf{q}_y^{(2)}(v_1)\otimes\mathbf{a}(\theta_1,\phi_1,\gamma_1,\eta_1),\cdots,\right.$
$\left.\mathbf{q}_x(u_K)\otimes\mathbf{q}_y^{(2)}(v_K)\otimes\mathbf{a}(\theta_K,\phi_K,\gamma_K,\eta_K)\right]$

$$\mathbf{q}_y^{(1)}(v_k) \stackrel{\text{def}}{=} \begin{bmatrix} e^{\frac{j2\pi\Delta_y 1v_k}{\lambda}} \\ \vdots \\ e^{\frac{j2\pi\Delta_y(M-1)v_k}{\lambda}} \end{bmatrix} \quad \mathbf{q}_y^{(2)}(v_k) \stackrel{\text{def}}{=} \begin{bmatrix} e^{\frac{j2\pi\Delta_y 2v_k}{\lambda}} \\ \vdots \\ e^{\frac{j2\pi\Delta_y Mv_k}{\lambda}} \end{bmatrix}$$

$$\tilde{\mathbf{I}}_1 \stackrel{\text{def}}{=} \left[\mathbf{I}_{3(M-1)} \vdots \mathbf{O}_3\right] \quad \tilde{\mathbf{I}}_2 \stackrel{\text{def}}{=} \left[\mathbf{O}_3 \vdots \mathbf{I}_{3(M-1)}\right] \tag{16}$$

In noiseless or asymptotic cases, the solution to the matrix equation $\mathbf{E}_1^v\mathbf{\Psi}^v = \mathbf{E}_2^v$ is $\mathbf{\Psi}^v = \mathbf{T}^{-1}\mathbf{\Phi}^v\mathbf{T}$, where $\mathbf{T}^v = \mathbf{P}^v\mathbf{T}$ and $\mathbf{P}^v$ is another unknown permutation matrix. Let the eigenvalues of $\mathbf{\Psi}^v$ be denoted $\nu_j$, $j = 1,\ldots,K$. It follows that

$$\nu_j = [\mathbf{\Phi}^v]_{jj} = e^{j\frac{2\pi}{\lambda}\Delta_y v_j}, \quad j = 1,\ldots,K \tag{17}$$

$$\mathbf{\Phi}^v = \text{diag}\left\{e^{j\frac{2\pi}{\lambda}\Delta_y v_1}, e^{j\frac{2\pi}{\lambda}\Delta_y v_2},\cdots,e^{j\frac{2\pi}{\lambda}\Delta_y v_K}\right\} \tag{18}$$

and the corresponding eigenvectors are the columns of $\mathbf{T}^{-1}$. With $\Delta_y$ greater than a half wavelength, the direction-cosine candidates of the $j$-th source relative to the $y$-axis are

$$\hat{v}_j^{(n_v)} = \nu_j + n_v\frac{\lambda}{\Delta_y}; \quad \nu_j = \frac{\angle[\mathbf{\Phi}^v]_{kk}}{2\pi\Delta_y/\lambda}$$

$$\left\lceil\frac{\Delta_x}{\lambda}(-1-\nu_j)\right\rceil \le n_v \le \left\lfloor\frac{\Delta_x}{\lambda}(1-\nu_j)\right\rfloor \tag{19}$$

(19) represents a set of of low-variance but ambiguous estimates of the direction-cosine relative to the $y$-axis.

#### *4.2.1. Pairing the Direction-Cosine Estimates:*

Note that different indices are used to enumerate the eigenvalues of $\mathbf{\Psi}^u$ and $\mathbf{\Psi}^v$ (i.e., the low-variance but cyclically ambiguous estimates of the direction-cosines $\{u_k, k = 1,\ldots,K\}$ and $\{v_j, j = 1,\ldots,K\}$) This is because even though $\mathbf{\Psi}^u$ and $\mathbf{\Psi}^v$ have common eigenvectors (in the noiseless or asymptotic cases), the ordering of the eigenvectors of $\mathbf{\Psi}^v$ will generally be permuted relative to the ordering of the eigenvectors of $\mathbf{\Psi}^u$ due to the presence of the unknown permutation matrices $\mathbf{P}^u$ and $\mathbf{P}^v$. In other words, the same set of eigenvectors is ordered differently in $(\mathbf{T}^u)^{-1}$ as in $(\mathbf{T}^v)^{-1}$. No mismatch, however, exists between $\mu_k$ and its corresponding eigenvector, which is simply the $k$-th column of $(\mathbf{T}^u)^{-1}$. Likewise, no mismatch exists between $\nu_j$ and its corresponding eigenvector, which is simply the $j$-th column of $(\mathbf{T}^v)^{-1}$. Thus, $\mu_k$ may be paired with $\nu_j$ from the same source by matching the orthogonal rows of $\mathbf{T}^u$ with those of $\mathbf{T}^v$ as follows. Let $(j_k, k)$ denote the row-index of the matrix element with the largest absolute value in the $k$-th column of the $K \times K$ matrix $\mathbf{T}^v(\mathbf{T}^u)^{-1}$. Then $\mu_k$ and $\nu_{j_k}$ belong to the same source. Note that this pairing procedure involves minimum computation and requires *no* exhaustive searches.

### 4.3. MUSIC-Based Disambiguation

After the overall element-space is decomposed into a $K$-dimensional signal subspace and a $(LM-K)$-dimensional noise subspace, MUSIC (MUltiple SIgnal Classification) [2] constructs a null spectrum parameterized by the signal parameters. Iterative search over this null spectrum for its $K$ deepest nulls would produce estimates of the $K$ sources' parameters.

MUSIC's null spectrum is constructed based on the orthogonality between the signal subspace and the noise subspace of the sample correlation matrix $\mathbf{R}_{xx}$. That is, $\mathbf{E}_s \perp \mathbf{E}_n$. Because $\mathbf{E}_s$ and $\mathbf{A}$ span the same column space, $\mathbf{A} \perp \mathbf{E}_n$. Recalling that $u$ and $v$ are both functions of $\{\theta, \phi\}$,

$$\{\hat{\theta}_k, \hat{\phi}_k\} = \underset{\{\theta,\phi\}}{\arg\min} \left\| \mathbf{E}_n^H \left(\mathbf{q}_x(u) \otimes \mathbf{q}_y(v) \otimes \mathbf{a}(\theta, \phi, \gamma, \eta)\right)\right\|$$

where the cost function above may be rewritten as:

$$\begin{aligned} &= [\mathbf{q}_x(u) \otimes \mathbf{q}_y(v) \otimes (\Phi(\theta,\phi)\mathbf{g}(\gamma,\eta))]^H \mathbf{E}_n \mathbf{E}_n^H \\ &\qquad [\mathbf{q}_x(u) \otimes \mathbf{q}_y(v) \otimes (\Phi(\theta,\phi)\mathbf{g}(\gamma,\eta))] \\ &= \left[(\mathbf{q}_x(u) \otimes \mathbf{q}_y(v))^H \otimes \left(\mathbf{g}(\gamma,\eta)^H \Phi(\theta,\phi)^H\right)\right] \mathbf{E}_n \mathbf{E}_n^H \\ &\qquad [\mathbf{q}_x(u) \otimes \mathbf{q}_y(v) \otimes (\Phi(\theta,\phi)\mathbf{g}(\gamma,\eta))] \\ &\qquad = \mathbf{g}(\gamma,\eta)^H \mathbf{M}(\theta,\phi)\mathbf{g}(\gamma,\eta) \end{aligned}$$

where

$$\begin{aligned} \mathbf{M}(\theta,\phi) \overset{def}{=} &\left[(\mathbf{q}_x(u) \otimes \mathbf{q}_y(v))^H \otimes \Phi(\theta,\phi)^H\right] \\ &\mathbf{E}_n \mathbf{E}_n^H \left[\mathbf{q}_x(u) \otimes \mathbf{q}_y(v) \otimes \Phi(\theta,\phi)\right] \end{aligned} \quad (20)$$

The identity $(\mathbf{M}_1\mathbf{M}_2)\otimes(\mathbf{M}_3\mathbf{M}_4) = (\mathbf{M}_1 \otimes \mathbf{M}_3)(\mathbf{M}_2 \otimes \mathbf{M}_4)$ is used in the preceding step. Noting that $\mathbf{M}(\theta,\phi)$ is a $2\times 2$ non-negative definite matrix,

$$\{\hat{\theta}_k, \hat{\phi}_k\} = \underset{\{\theta,\phi\}}{\arg\min} \{\text{smallest eigenvalue of } \mathbf{M}(\theta,\phi)\} \quad (21)$$

Thus, the direction-finding problem is again decoupled from the polarization estimation problem.

Note that this MUSIC-based disambiguation step renders it unnecessary to use the vector cross-product estimator to derive any coarse reference estimates. Thus, it becomes no longer necessary to have all available all six electromagnetic components of the impinging wavefront. It would be sufficient to have available as few as only any two of the six electromagnetic components, because the resulting array manifold would still retain its one-to-one relation with the impinging source's direction cosine. The cyclically ambiguous set of direction cosines along the x-axis may be aligned with the set along the y-axis by methods such as that presented in [8].

While the present MUSIC step may be applied to arrays of any geometry, the uniformly spaced configuration used in the present algorithm minimizes the support region of MUSIC's iterative search from a continuous region $\{0 \le \theta < \pi, 0 \le \phi < 2\pi\}$ to a small finite set of discrete points:

$$\left\{\hat{u}_k(n_u), \hat{v}_k(n_v), \quad \text{for } \left\lceil \frac{\Delta_x}{\lambda}(-1-\mu_k)\right\rceil \le n_u \le \left\lfloor \frac{\Delta_x}{\lambda}(1-\mu_k)\right\rfloor, \left\lceil \frac{\Delta_y}{\lambda}(-1-\nu_k)\right\rceil \le n_v \le \left\lfloor \frac{\Delta_y}{\lambda}(1-\nu_k)\right\rfloor\right\}$$

## 5. SIMULATIONS

Simulation results in Figures 1 to 4 verify the efficacy of the proposed extended aperture concept using sparsely spaced dipoles and/or loops. The wireless mobile fading channel is modeled as slow-fading and frequency-selective. For illustration, present simulations use a two-multipath model. The source is a BPSK sequence modulated by the raised-cosine waveform with $\beta = 0.35$. The two multipaths, with timing offset equals 0.3 of a symbol period, impinge upon a $4 \times 4$ rectangular array of identically oriented dipole-triads equi-spaced at 8 wavelengths. Each dipole triad consists of three co-located but orthogonally oriented identical dipoles. The multipath parameters were: $u_1 = 0.61, v_1 = 0.79, \gamma_1 = 45°, \eta_1 = -90°, \mathcal{P}_1 = 1, u_1 = 0.69, v_2 = 0.71, \gamma_2 = 45°, \eta_2 = 90°, \mathcal{P}_2 = 0.7079$. 50 symbols are sampled at 10 samples per symbol in each experiment; and there are 100 experiments per data point. Spatial smoothing performed by forming four $3 \times 3$ dipole-triad subarrays. For comparison, the same scenario is used with a $7 \times 7$ half-wavelength spaced omni-directional scalar-sensor array, where spatial-smoothing [3] is performed using four $6 \times 6$ subarrays. A scalar sensor refers to the situation where each dipole-triad is replaced by a scalar-sensor which measures the Frobenius norm of the Poynting vector. This $7 \times 7$ half-wavelength spaced scalar-sensor array has an array manifold size comparable to the $4 \times 4$ extended-aperture dipole-triad array.

Referring to figures 1 and 2, the present extended-aperture algorithm clearly offers significantly lower estimation standard deviations and biases than the half-wavelength-spaced scalar-sensor array at all SNR. Because the two multipaths' direction-cosines are separated by 0.08, the two multipaths may be considered as resolved when their estimation standard deviations fall below 0.01. Using this criteria, the proposed scheme has a resolution threshold below $-10$ dB compared to about 0 dB for the half-wavelength spaced scalar-sensor array. In the SNR $> 0$ dB range where the standard deviation and bias of both arrays fall off rather linearly with increasing SNR, the proposed method offers almost *one and a half orders of magnitude* reduction in standard deviation and about an order of magnitude reduction in bias.

In figures 3 and 4, the SNR becomes set at 0 dB while the multipaths' relative timing offset is varied. Again, the present extended-aperture algorithm clearly offers significantly lower estimation standard deviations and biases than the half-wavelength-spaced scalar-sensor array at all timing offsets. The scalar-sensor array, despite spatial smoothing, fails to resolve the two multi-paths for timing offset below 0.3 of a symbol period. In contrast, the proposed scheme offers near identical error statistics to all timing offset. In the timing offset range greater than 0.5 of a symbol period, where the half-wavelength spaced scalar-sensor array's error statistics level off, the proposed scheme outperform the half-wavelength spaced scalar-sensor array, offering about *an order of magnitude* reduction in standard deviation and bias.

When all six electromagnetic field components are to be separately measured, (for example by a "vector sensor" comprising three orthogonally oriented dipoles plus three orthogonally oriented loops, all co-located in space,) then an alternative disambiguation approach is realizable by applying a vector cross-product between the electric-field components and the magnetic-field components. For details, please refer to [5,6]. An underwater acoustic analog of the present algorithm is introduced by the present authors in [7]. Another extended-aperture algorithm, applicable to any propagation medium, is presented also by the present authors in [8] using dual-size spatial invariances.

## 6. REFERENCES


[1] W. C. Y. Lee & S. Y. Yeh, "Polarizational Diversity System for Mobile Radio," *IEEE Trans. Communications*, pp 912-922, Oct. 1972.

[2] R. O. Schmidt, " Multiple Emitter Location and Signal Parameter Estimation". *Proc. RADC Spectral Estimation*

*Workshop*, Griffiss AFBS, NY, 1979.
[3] T. J. Shan, M. Wax & T. Kailath, "On Spatial Smoothing for Direction-of-Arrival Estimation of Coherent Signals," *IEEE Trans. Acoustics, Speech, Signal Processing*, vol. 33, no. 8, pp. 806-811, Aug. 1985.
[4] R. Roy & T. Kailath, "ESPRIT-Estimation of Signal Parameters Via Rotational Invariance Techniques," *IEEE Trans. Acoustics, Speech, Signal Processing*, vol. 37, no. 7, pp. 984-995, Jul. 1989.
[5] K. T. Wong & M. D. Zoltowski, "ESPRIT-Based 2D Angle Estimation with Extended Aperture Electromagnetic Vector-Sensor Arrays," *IEEE Intl. Conf. Acoustics, Speech & Signal Processing 1996*, vol. 5, pp. 2789-2792.
[6] M. D. Zoltowski & K. T. Wong, "Closed-form ESPRIT-based 2D Direction-Finding with an Extended-Aperture Array of Electromagnetic Vector-Sensors," submitted to *IEEE Trans. Signal Processing.*
[7] K. T. Wong & M. D. Zoltowski, "ESPRIT-Based Extended-Aperture Source Localization Using Velocity-Hydrophones," *MTS/IEEE Oceans 96 Conf.*, vol. 3, pp. 1427-1432.
[8] K. T. Wong & M. D. Zoltowski, "Sparse Array with Dual-Size Spatial Invariances for Extended-Aperture ESPRIT-Based Direction Finding," in press, *1996 IEEE Midwest Symp. on Circuits & Systems.*

Figure 1: RMS standard deviation of $\{\hat{u}_1, \hat{v}_1, \hat{u}_2, \hat{v}_2\}$, vs. SNR:

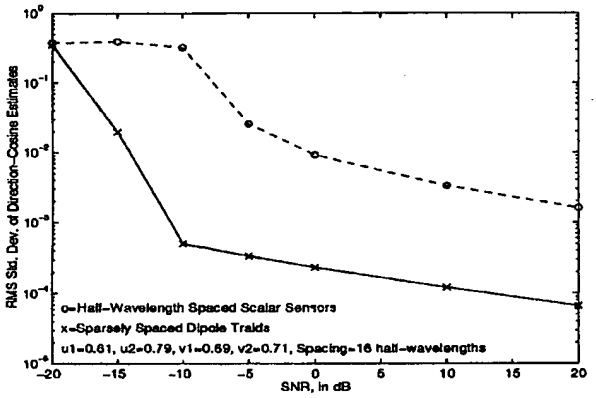


Figure 2: RMS Bias of $\{\hat{u}_1, \hat{v}_1, \hat{u}_2, \hat{v}_2\}$, vs. SNR. All parameters are identical with those in Figure 1.

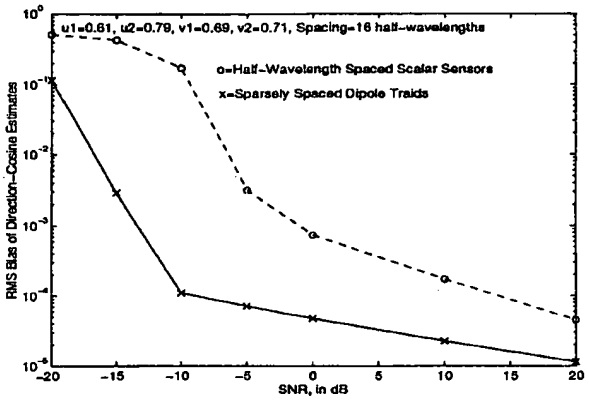


Figure 3: RMS standard deviation of $\{\hat{u}_1, \hat{v}_1, \hat{u}_2, \hat{v}_2\}$ vs. timing offset, SNR with respect to first multi-path is 0 dB, all other parameters same as in figure 1.

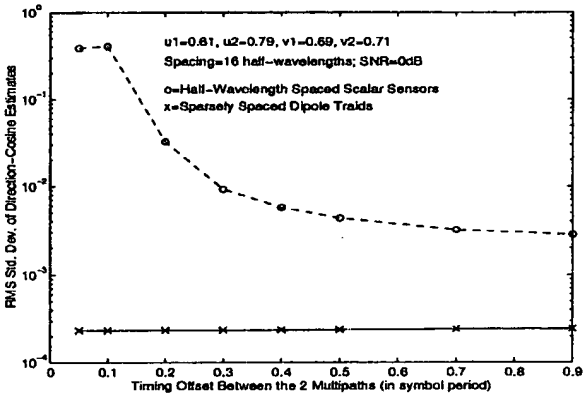


Figure 4: RMS Bias of $\{\hat{u}_1, \hat{v}_1, \hat{u}_2, \hat{v}_2\}$ vs. timing offset, all parameters are same as in figure 3.

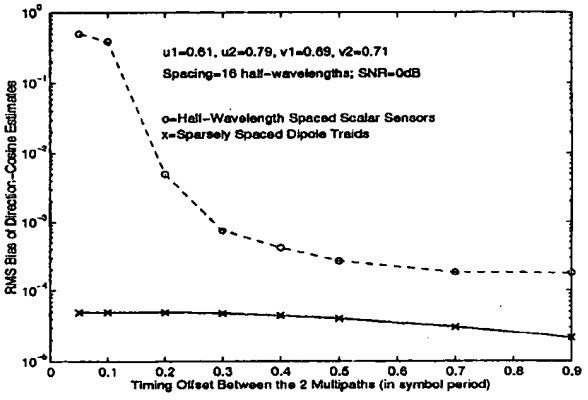

# High accuracy 2D angle estimation with extended aperture vector sensor arrays

Wong, K.T. Zoltowski, M.D.
Dept. of Electr. & Comput. Eng., Purdue Univ., West Lafayette, IN;

*This paper appears in:* **Acoustics, Speech, and Signal Processing, 1996. ICASSP-96. Conference Proceedings., 1996 IEEE International Conference on**
05/07/1996 -05/10/1996, 7-10 May 1996
Location: Atlanta, GA , USA
On page(s): 2789-2792 vol. 5
Volume: 5, 7-10 May 1996
References Cited: 4
Number of Pages: 6 vol. lvii+3588
INSPEC Accession Number: 5490265

**Abstract:**
A novel ESPRIT-based 2D angle estimation scheme is proposed involving the use of a right-triangular array of three vector sensors spaced much farther apart than a half-wavelength. A vector sensor is composed of six co-located antennas distinctly measuring all six electromagnetic field components of a multi-component incident wavefield. Information on each source's respective electromagnetic field components is obtained by decoupling the signal eigenvectors via lower dimensional eigenvectors derived from TLS-ESPRIT. This facilitates estimation of each source's respective Poynting vector thereby enabling one to resolve the phase ambiguities in ESPRIT's eigenvalues when the intervector-sensor spacing is greater than a half-wavelength. Simulations are presented showing the sample variance of the direction cosine estimates decreasing linearly on a log-log scale as the intervector-sensor spacing is increased from a half-wavelength to 30 wavelengths, with a factor of 80 reduction in the latter case relative to the former case. The proposed scheme and attendant vector sensor array also outperform a uniformly-spaced array of scalar sensors with the same aperture and same number of component antennas whenever the intervector sensor spacing in the former case is greater than 3 half-wavelengths

**Index Terms:**
array signal processing direction-of-arrival estimation eigenvalues and eigenfunctions signal resolution ESPRIT based 2D angle estimation Poynting vector TLS-ESPRIT array resolution colocated antennas direction cosine estimates eigenvectors electromagnetic field components extended aperture vector sensor arrays half wavelength high accuracy 2D angle estimation intervector-sensor spacing multicomponent incident wavefield phase ambiguities right triangular array sample variance scalar sensors signal eigenvectors simulations uniformly spaced array

# High Accuracy 2D Angle Estimation With Extended Aperture Vector Sensor Arrays †

Kainam T. Wong
kainam@ecn.purdue.edu

Michael D. Zoltowski
mikedz@ecn.purdue.edu

School of Electrical and Computer Engineering
Purdue University
W. Lafayette, IN 47907-1285 U.S.A.

## ABSTRACT

A novel ESPRIT-based 2D angle estimation scheme is proposed involving the use of a right-triangular array of three vector sensors spaced much farther apart than a half-wavelength. A vector sensor is composed of six co-located antennas distinctly measuring all six electromagnetic field components of a multi-component incident wavefield. Information on each source's respective electromagnetic field components is obtained by decoupling the signal eigenvectors via lower dimensional eigenvectors derived from TLS-ESPRIT. This facilitates estimation of each source's respective Poynting vector thereby enabling one to resolve the phase ambiguities in ESPRIT's eigenvalues when the inter-vector-sensor spacing is greater than a half-wavelength. Simulations are presented showing the sample variance of the direction cosine estimates decreasing linearly on a log-log scale as the inter-vector-sensor spacing is increased from a half-wavelength to 30 wavelengths, with a factor of 80 reduction in the latter case relative to the former case. The proposed scheme and attendant vector sensor array also outperform a uniformly-spaced array of scalar sensors with the same aperture and same number of component antennas whenever the inter-vector sensor spacing in the former case is greater than 3 half-wavelengths.

## 1. INTRODUCTION

Array resolution and accuracy are limited by the effective size of the array aperture. In general, a larger array aperture yields correspondingly more accurate DOA estimates [1]. The array aperture may be enlarged by adding more antenna elements in the case of uniform half-wavelength spacing, by spacing the elements nonuniformly over a larger aperture, or by increasing the separation between elements in the case of uniform spacing. Adding more antennas has the obvious drawbacks of increasing hardware costs plus expanding the already considerable computational load required by eigenstructure methods. Nonuniform inter-element spacing would generally violate ESPRIT's requirement of two identical but translated subarrays. The spatial version of the Nyquist Sampling Theorem also poses an upper limit on the distance between elements in the case of uniform spacing without causing aliasing. Two identical sensors spaced over a half-wavelength apart will lead to a set of ambiguous direction-cosine estimates. With no a-priori information, this ambiguity cannot be resolved using unpolarized scalar sensors.

A novel scheme is proposed employing a sparse array of six-component electromagnetic vector-sensors [2] that is able to resolve the aforementioned ambiguity despite inter-vector sensor spacings much greater than a half-wavelength. Exceptional estimation accuracy is facilitated by a large effective aperture and exploitation of differences in sources' respective polarizations.

### 1.1. Basic Principles Underlying New Algorithm

A vector-sensor consists of six spatially co-located antennas measuring all three electrical-field components and all three magnetic-field components of the incident wave-field [2]. The proposed array geometry is that of three vector-sensors located at $(0,0)$, $(\Delta,0)$, and $(0,\Delta)$ in $(x,y)$ Cartesian coordinates. The inter-vector sensor spacing $\Delta$ is assumed to be much greater than a half-wavelength to effect a large array aperture and correspondingly achieve highly accurate source direction estimates. A pair of identical vector-sensors effectively represent two identical six-element subarrays displaced in space thereby facilitating the use of ESPRIT [3]. TLS-ESPRIT is applied to the data from the vector sensors located at $(0,0)$ and $(\Delta,0)$ to ultimately yield estimates of the direction cosine of each source relative to the x-axis, $\{u_k = \cos\phi_k \sin\theta_k, \quad k = 1,\ldots,K\}$, where $\phi_k$ and $\theta_k$ are the azimuth and elevation arrival angles of the $k$-th incident signal. Simultaneously, TLS-ESPRIT is applied to the data from the vector sensors located at $(0,0)$ and $(0,\Delta)$ to ultimately yield estimates of the direction cosine of each source relative to the $y$-axis, $\{v_k = \cos\phi_k \sin\theta_k, \quad k = 1,\ldots,K\}$.

However, when the inter-vector sensor spacing is greater than a half-wavelength there is an integer multiple of $2\pi$ ambiguity in the phase of each eigenvalue generated in the final stage of TLS-ESPRIT. This leads to ambiguous DOA estimates equi-spaced by $\lambda/\Delta$ in the interval $-1 \le u_k < 1$ (or $-1 \le v_k < 1$ as the case may be.) If one could resolve this ambiguity, the resulting DOA estimate would be highly accurate due to the large aperture. The key idea of this paper is to use the Poynting vector information for each source embedded in the output of each vector sensor to resolve this ambiguity. The lower dimensional eigenvectors generated in the final stage of TLS-ESPRIT are used to decouple the element space signal eigenvectors to yield both the electric field vector and the magnetic field vector for each source. The cross product between these two vectors for a given source yields the Poynting vector for that source. Normalizing the Poynting vector for a given source to have unit length, its components are the direction cosines of that source relative to the $x$, $y$, and $z$ axes. That is,

$$\mathbf{p}_k \stackrel{\text{def}}{=} \begin{bmatrix} p_{x_k} \\ p_{y_k} \\ p_{z_k} \end{bmatrix} = \begin{bmatrix} u_k \\ v_k \\ w_k \end{bmatrix}$$

$$= \mathrm{Re}\left\{ \frac{\mathbf{e}(\theta_k,\phi_k,\gamma_k,\eta_k)}{\|\mathbf{e}(\theta_k,\phi_k,\gamma_k,\eta_k)\|} \times \frac{\mathbf{h}^*(\theta_k,\phi_k,\gamma_k,\eta_k)}{\|\mathbf{h}(\theta_k,\phi_k,\gamma_k,\eta_k)\|} \right\} \quad (1)$$

†This research was supported by the Air Force Office of Scientific Research under grant no. F49620-95-1-0367, the National Science Foundation under under grant no. MIPS-9320890, and the Army Research Office's Focused Research Initiative under grant number DAAHO4-95-1-0246.

0-7803-3192-3/96 $5.00©1996 IEEE

where $w_k = \sqrt{1-u_k^2-v_k^2}$, $*$ denotes conjugation, and $\gamma_k$ and $\eta_k$ are polarization parameters defined in Section 2. The idea is to use these as "coarse" estimates to resolve the integer multiple of $\lambda/\Delta$ ambiguity in the DOA estimates yielded by TLS-ESPRIT's eigenvalues.

The direction cosine estimates produced by the Poynting vector estimation procedure are characterized as high variance but unambiguous in comparison to the direction cosine estimates extracted from the TLS-ESPRIT eigenvalues which are characterized as low variance but ambiguous. Intuitively, the lower variance of the latter relative to the former is due to the fact that the direction cosine estimates extracted from the TLS-ESPRIT eigenvalues depend on the size of the array aperture as measured by $\Delta$: the larger $\Delta$, the smaller the variance of $\angle\hat{\mu}_k/2\pi\Delta$, where $\hat{\mu}_k$ is a TLS-ESPRIT eigenvalue associated with the $k$-th source. This is confirmed by simulations presented in Section 4. The relative high variance of the direction cosine estimates extracted from the Poynting vector estimates is intuitively due to the fact that they are inherently extracted from information provided by a single vector sensor which has no effective aperture.

## 2. VECTOR SENSOR ARRAY DATA MODEL

The propagation model is transverse electromagnetic planewaves traveling through a non-conductive homogeneous isotropic medium. Under these conditions, the wavefront incident upon the array has an electric-field vector, e, and corresponding magnetic-field vector, h, that can be expressed in Cartesian coordinates as [2]

$$\begin{aligned}\mathbf{e} &= e_x\vec{v}_x + e_y\vec{v}_y + e_z\vec{v}_z \qquad (2)\\ &= (sin\gamma\, cos\theta\, cos\phi\, e^{j\eta} - cos\gamma\, sin\phi)\vec{v}_x \\ &\quad +(sin\gamma\, cos\theta\, sin\phi\, e^{j\eta} + cos\gamma\, cos\phi)\vec{v}_y \\ &\quad -sin\gamma\, sin\theta\, e^{j\eta}\vec{v}_z \qquad (3)\\ \mathbf{h} &= h_x\vec{v}_x + h_y\vec{v}_y + h_z\vec{v}_z \qquad (4)\\ &= -(cos\gamma\, cos\theta\, cos\phi + sin\gamma\, sin\phi\, e^{j\eta})\, Z_o\vec{v}_x \\ &\quad -(cos\gamma\, cos\theta\, sin\phi - sin\gamma\, cos\phi\, e^{j\eta})\, Z_o\vec{v}_y \\ &\quad +cos\gamma\, sin\theta\, Z_o\vec{v}_z \qquad (5)\end{aligned}$$

where $0 \le \gamma \le \pi/2$ is the auxiliary polarization angle, $-\pi \le \eta \le \pi$ is the polarization phase difference, $0 \le \theta \le \pi$ is the signal's elevation angle measured from the vertical $z$-axis, $0 \le \phi \le 2\pi$ is the azimuth angle, $Z_o$ is the transmission medium's intrinsic impedance, and $\vec{v}$ is a unit-vector along the coordinate specified by its subscript.

$K$ co-channel signal sources are assumed to be in the far field and narrowband in the sense that the bandwidth is very small relative to the carrier frequency. Given a right-triangular array of three vector sensors with the geometry described previously, the $18 \times 1$ snapshot vector at time $t$ may be expressed as

$$\mathbf{z}(t) = \sum_{k=1}^{K} s_k(t)e^{j\omega_c t}\mathbf{v}(\theta_k,\phi_k)\otimes\mathbf{a}(\theta_k,\phi_k,\gamma_k,\eta_k) + \mathbf{n}(t). \quad (6)$$

The first. middle, and last $6 \times 1$ sub-vectors of $\mathbf{z}(t)$ are the outputs of the six component-antennas comprising the vector sensor located at the Cartesian coordinates $(0,0)$, $(\Delta,0)$, and $(0,\Delta)$, respectively, relative to the $x-y$ plane. The various quantities are defined as follows. $\mathbf{v}(\theta_k,\phi_k)$ is the $3 \times 1$ manifold describing the relative phases between vector sensors for the $k$-th source due to the propagation delays

$$\mathbf{v}(\theta_k,\phi_k) = \begin{bmatrix} 1 \\ e^{j\frac{2\pi}{\lambda}\Delta u_k} \\ e^{j\frac{2\pi}{\lambda}\Delta v_k} \end{bmatrix} \qquad (7)$$

where $\lambda$ is the wavelength associated with the center frequency, $\omega_c$, of the passband of the front end bandpass filter. $\otimes$ is the Kronecker product. $\mathbf{a}_k \stackrel{\text{def}}{=} \mathbf{a}(\theta_k,\phi_k,\gamma_k,\eta_k)$ is the $6 \times 1$ composite electromagnetic field vector for the $k$-th source sensed at each vector sensor, *i.e.*,

$$\mathbf{a}_k = \begin{bmatrix} e_{x_k} \\ e_{y_k} \\ e_{z_k} \\ h_{x_k} \\ h_{y_k} \\ h_{z_k} \end{bmatrix} = \begin{bmatrix} sin\gamma_k cos\theta_k cos\phi_k e^{j\eta_k} - cos\gamma_k sin\phi_k \\ sin\gamma_k cos\theta_k sin\phi_k e^{j\eta_k} + cos\gamma_k cos\phi_k \\ -sin\gamma_k sin\theta_k e^{j\eta_k} \\ (-cos\gamma_k cos\theta_k cos\phi_k - sin\gamma_k sin\phi_k e^{j\eta_k})Z_o \\ (-cos\gamma_k cos\theta_k sin\phi_k + sin\gamma_k cos\phi_k e^{j\eta_k})Z_o \\ (cos\gamma_k sin\theta_k)Z_o \end{bmatrix} \qquad (8)$$

$s_k(t)$ is the complex baseband signal comprising the $k$-th signal arrival. Finally, $\mathbf{n}(t)$ is an $18 \times 1$ additive noise vector.

## 3. 2D ANGLE ESTIMATION VIA AN EXTENDED APERTURE VECTOR SENSOR ARRAY

### 3.1. Adapting ESPRIT to Vector Sensor Arrays

ESPRIT [1] is applicable to the right triangular array of three vector sensors because any two vector sensors represents a pair of identical six element subarrays. The first step in ESPRIT is to compute the signal eigenvectors. Let $\hat{\mathbf{E}}_S$ be an $18 \times K$ matrix composed of the $K$ "largest" eigenvectors of the $18 \times 18$ sample covariance matrix

$$\hat{\mathbf{R}}_{zz} = \frac{1}{N}\sum_{i=1}^{N}\mathbf{z}(t_i)\mathbf{z}^H(t_i).$$

Due to the invariance associated with the two vector sensors along the $y$-axis as well as the invariance associated with the two vector sensors along the $x$-axis, it follows from the snapshot model in (6), that $\hat{\mathbf{E}}_S$ asymptotically approaches the following form

$$\mathbf{E}_S = \begin{bmatrix} \mathbf{E}_1 \\ \mathbf{E}_2 \\ \mathbf{E}_3 \end{bmatrix} = \mathbf{AT} = \begin{bmatrix} \mathbf{A}_1 \\ \mathbf{A}_1\Phi^u \\ \mathbf{A}_1\Phi^v \end{bmatrix}\mathbf{T}, \qquad (9)$$

where $\mathbf{A}_1$ is the $6 \times K$ matrix

$$\mathbf{A}_1 = [\mathbf{a}_1,\mathbf{a}_2,...,\mathbf{a}_K] = \begin{bmatrix} \mathbf{e}_1 & \mathbf{e}_2 & ... & \mathbf{e}_K \\ \mathbf{h}_1 & \mathbf{h}_2 & ... & \mathbf{h}_K \end{bmatrix}, \qquad (10)$$

$\Phi^u$ and $\Phi^v$ are the $K \times K$ diagonal matrices,

$$\Phi^u = \text{diag}\left\{e^{j\frac{2\pi}{\lambda}\Delta u_1}, e^{j\frac{2\pi}{\lambda}\Delta u_2}, ..., e^{j\frac{2\pi}{\lambda}\Delta u_K}\right\}, \qquad (11)$$

$$\Phi^v = \text{diag}\left\{e^{j\frac{2\pi}{\lambda}\Delta v_1}, e^{j\frac{2\pi}{\lambda}\Delta v_2}, ..., e^{j\frac{2\pi}{\lambda}\Delta v_K}\right\}, \qquad (12)$$

respectively, and $\mathbf{T}$ is an unknown $K \times K$ matrix.

It is easily shown that in the no noise or asymptotic cases the solution to the matrix equation $\hat{\mathbf{E}}_1\hat{\Psi}^u = \hat{\mathbf{E}}_2$ is $\Psi^u = \mathbf{T}^{-1}\Phi^u\mathbf{T}$. Let the eigenvalues of $\Psi^u$ be denoted $\mu_k$, $k = 1,...,K$. It follows that $\mu_k = \Psi^u_{kk} = e^{j\frac{2\pi}{\lambda}\Delta u_k}$, $k = 1,...,K$, and the corresponding eigenvectors are the columns of $\mathbf{T}^{-1}$. If the inter-vector sensor spacing $\Delta$ is greater than a half wavelength, the candidates for the direction cosine of the $k$-th source relative to the $x$-axis are

$$\hat{u}_k^{(m)} = \frac{\lambda}{2\pi\Delta}\angle\hat{\mu}_k + m\frac{\lambda}{\Delta}, \left\lceil -\frac{\Delta}{\lambda} - \frac{\angle\hat{\mu}_k}{2\pi}\right\rceil \le m \le \left\lfloor \frac{\Delta}{\lambda} - \frac{\angle\hat{\mu}_k}{2\pi}\right\rfloor \qquad (13)$$

where $\angle\hat{\mu}_k$ is the principal argument of $\hat{\mu}_k$ in the range $-\pi < \angle\hat{\mu}_k \le \pi$, $\lceil x \rceil$ is the closest integer to $x$ that is greater

than $x$, and $\lfloor x \rfloor$ is the closest integer to $x$ that is less than $x$. (13) represents a set of of low variance but ambiguous estimates of the direction cosine of the $k$-th source relative to the $x$-axis.

Similarly, in the asymptotic or no noise cases the solution to the matrix equation $\hat{\mathbf{E}}_1\hat{\Psi}^v = \hat{\mathbf{E}}_3$ is $\Psi^v = \mathbf{T}^{-1}\Phi^v\mathbf{T}$. Let the eigenvalues of $\Psi^v$ be denoted $\nu_\ell$, $\ell = 1,...,K$. It follows that $\nu_\ell = \Psi^v_{\ell\ell} = e^{j\frac{2\pi}{\lambda}\Delta v_\ell}$, $\ell = 1,...,K$, and the corresponding eigenvectors are the columns of $\mathbf{T}^{-1}$. With $\Delta$ greater than a half wavelength, the candidates for the direction cosine of the $\ell$-th source relative to the $y$-axis are

$$\hat{v}_\ell^{(n)} = \frac{\lambda}{2\pi\Delta}\angle\hat{\nu}_\ell + n\frac{\lambda}{\Delta}, \quad \left\lceil -\frac{\Delta}{\lambda} - \frac{\angle\hat{\nu}_k}{2\pi} \right\rceil \le n \le \left\lfloor \frac{\Delta}{\lambda} - \frac{\angle\hat{\nu}_k}{2\pi} \right\rfloor \tag{14}$$

(14) represents a set of of low variance but ambiguous estimates of the direction cosine of the $k$-th source relative to the $y$-axis.

Note that different indices are used to enumerate the respective eigenvalues of $\hat{\Psi}^u$ and $\hat{\Psi}^v$. Although $\Psi^u$ and $\Psi^v$ have common eigenvectors, the ordering of the eigenvectors of $\Psi^v$ will in general be permuted relative to the ordering of the eigenvectors of $\Psi^u$. van der Veen *et al* [4] have developed a 2D extension of ESPRIT that exploits the fact that $\Psi^u$ and $\Psi^v$ commute, since they have common eigenvectors, to automatically pair the eigenvalues of $\Psi^u$ with those of $\Psi^v$ so that each resulting pair of eigenvalues is one-to-one associated with an incident wavefront thereby automatically pairing the direction cosine estimates with respect to the two array axes.

Effectively, van der Veen *et al* propose a scheme for perturbing both $\hat{\Psi}^u$ and $\hat{\Psi}^v$ so that the resulting perturbed matrices commute. $\hat{\mathbf{T}}^{-1}$ is then constructed from the eigenvectors of either perturbed matrix. Pre- and post-multiplying both the perturbed $\hat{\Psi}^u$ and the perturbed $\hat{\Psi}^v$ by $\hat{\mathbf{T}}$ and $\hat{\mathbf{T}}^{-1}$, respectively, yields a pair of approximately diagonal matrices whose diagonal elements are automatically paired[1]. At this point, we will assume that the respective eigenvalues of $\hat{\Psi}^u$ and $\hat{\Psi}^v$ have been correctly paired.

The matrix whose columns are one-to-one related to the electromagnetic field vectors for each source defined by (10) may be estimated as

$$\hat{\mathbf{A}}_1 = \frac{1}{3}\left\{\hat{\mathbf{E}}_1\hat{\mathbf{T}}^{-1} + \hat{\mathbf{E}}_2\hat{\mathbf{T}}^{-1}\hat{\Phi}^{u*} + \hat{\mathbf{E}}_3\hat{\mathbf{T}}^{-1}\hat{\Phi}^{v*}\right\} \tag{15}$$

Now, since the $k$-th column of $\hat{\mathbf{T}}^{-1}$ is the eigenvector associated with the $k$-th eigenvalue of $\hat{\Psi}^u$, $\hat{\mu}_k$, the $k$-th column of $\hat{\mathbf{A}}_1$ above is associated with $\hat{\mu}_k$. Given the expression for the asymptotic form of $\hat{\mathbf{A}}_1$ in the far right hand side of (10), the Poynting vector for the $k$-th source may be estimated via the vector cross-product between the top and bottom $3 \times 1$ subvectors of the $k$-th column of $\hat{\mathbf{A}}_1$ according to (1). Normalizing the resulting cross-product vector to have unit length, the first and second components are high-variance but unambiguous estimates of the direction cosine of the $k$-th source relative to the $x$ and $y$ axes, respectively.

### 3.2. Disambiguation of ESPRIT Eigenvalues

Let $\hat{\mathbf{p}} = [\hat{p}_{x_k}, \hat{p}_{y_k}, \hat{p}_{z_k}]^T$ denote the estimate of the normalized Poynting vector obtained by using the eigenvectors of the perturbed $\hat{\Psi}^u$ to decouple the signal eigenvectors comprising $\hat{\mathbf{E}}_S$ and the subsequent column-wise vector cross product vector as described above. The first two components of this vector are used as coarse estimates to disambiguate the candidate estimates of $u_k$ and $v_\ell$ described by (13) and (14), respectively. The disambiguated estimates are

$$\hat{u}_k = \frac{\lambda}{2\pi\Delta}\angle\hat{\mu}_k + m^\circ\frac{\lambda}{\Delta} \quad \text{and} \quad \hat{v}_k = \frac{\lambda}{2\pi\Delta}\angle\hat{\nu}_k + n^\circ\frac{\lambda}{\Delta}$$

where $m^\circ$ and $n^\circ$ may be jointly estimated as
Method 1:

$$\{m^\circ, n^\circ\} \stackrel{\text{def}}{=} \arg\left[\min \left\|\begin{bmatrix} \hat{p}_{x_k} - \frac{\lambda}{2\pi\Delta}\angle\hat{\mu}_k - \frac{m\lambda}{\Delta} \\ \hat{p}_{y_k} - \frac{\lambda}{2\pi\Delta}\angle\hat{\nu}_k - \frac{n\lambda}{\Delta} \end{bmatrix}\right\|\right] \tag{16}$$

where $\|\ \|$ denotes the Frobenius norm, or estimated individually as
Method 2:

$$m^\circ \stackrel{\text{def}}{=} \arg\left[\min \left|\hat{p}_{x_k} - \frac{\lambda}{2\pi\Delta}\angle\hat{\mu}_k - \frac{m\lambda}{\Delta}\right|\right]$$
$$n^\circ \stackrel{\text{def}}{=} \arg\left[\min \left|\hat{p}_{y_k} - \frac{\lambda}{2\pi\Delta}\angle\hat{\nu}_k - \frac{m\lambda}{\Delta}\right|\right] \tag{17}$$

The search range for $m$ and $n$ in both cases is given by the far right hand side of (13) and (14), respectively.

Method I tests up to a maximum of $\lfloor 2\frac{\Delta}{\lambda} + 1 \rfloor^2$ candidate pairs, whereas Method II only tests up to a maximum of $2\lfloor 2\frac{\Delta}{\lambda} + 1 \rfloor$ candidates. Although Method II is computationally more efficient, it determines $m^\circ$ and $n^\circ$ in a separable manner and may thus yield "worst" estimates relative to the jointly based technique signified by Method I. However, simulations of both methods have revealed no difference in their respective estimates when the inter-vector sensor spacing $\Delta$ is below a certain threshold.

## 4. SIMULATIONS

Simulation results presented in Figures 1 and 2 verify the efficacy of the extended aperture vector sensor array concept and attendant ESPRIT-based 2D angle estimation algorithm. The signal scenario involved two uncorrelated sources with the following location and polarization parameters: $\theta_1 = 41.4°, \phi_1 = 36.0°, \gamma_1 = 18°, \eta_1 = -54°$, $\theta_2 = 66.6°, \phi_2 = 46.8°, \gamma_2 = 72°, \eta_2 = 126°$. The SNR per component antenna was 20 dB for source 1 and 17 dB for source 2. For a given trial run, the $18 \times 18$ sample correlation matrix was formed from $N = 32$ snapshots.

For each different value of the inter-vector sensor spacing, $\Delta$, sample biases and sample variances for both $\hat{u}_k$ and $\hat{v}_k$, $k = 1, 2$, were computed for each of the two sources from 300 independent trial runs. For a given source, an RMS standard deviation was computed by taking the square root of the sum of the respective samples variances for $\hat{u}_k$ and $\hat{v}_k$. An RMS bias was also computed by taking the square root of the sum of the respective sample biases for $\hat{u}_k$ and $\hat{v}_k$. Figure 1 shows the RMS standard deviation for source 1 as $\Delta$ is increased from a half-wavelength to over 50 wavelengths (100 half-wavelengths.) On a log-log scale it is observed that the RMS std. dev. decreases linearly as the inter-vector sensor spacing is increased from a half-wavelength up to 32 wavelengths, at which point there is a factor of 80 reduction relative to the RMS std. dev. obtained with half-wavelength inter-vector sensor spacing. The RMS bias for source 1 plotted in Figure 2 exhibits a similar behavior and is an order of magnitude lower than the RMS std. dev. Note that the RMS std. dev. and RMS bias curves for source 2 are very nearly identical to that for source 1 but are not included here due to space limitations.

Figures 1 and 2 also show the RMS standard deviation and RMS bias of the direction cosine estimates for source

[1] In actuality, van der Veen *et al* employ a Schur decomposition as opposed to an EVD and there is much detail on how they approximately enforce commutativity that is not included here due to space limitations.

1 obtained by the Poynting vector estimation procedure proposed in this paper. Both curves are observed to be relatively constant as the inter-vector sensor spacing is increased from $\Delta = \lambda/2$ to $\Delta = 32\lambda$. Both curves are observed to be well above the corresponding counterpart curves associated with the disambiguated direction cosine estimates, with the separation between the two widening as the inter-vector sensor spacing is increased from $\Delta = \lambda/2$ to $\Delta = 32\lambda$. This substantiates the claim that the Poynting vector estimation procedure yields high-variance but unambiguous direction cosine estimates in comparison to the direction cosine estimates extracted from TLS-ESPRIT's eigenvalues according to (13) and (14). Intuitively, the lower variance of the latter relative to the former is due to the fact that the direction cosine estimates extracted from the TLS-ESPRIT's eigenvalues depend on the size of the array aperture as measured by $\Delta$: the larger $\Delta$, the smaller the variance of $\angle\hat{\mu}_k/2\pi\Delta$. The relative high variance of the direction cosine estimates extracted from the Poynting vector estimates is intuitively due to the fact that they are inherently extracted from information provided by a single vector sensor which has no effective aperture.

A breakdown phenomenon is observed at a threshold inter-vector sensor spacing of $\Delta = 32\lambda$ (64 half-wavelengths.) The cause of this breakdown is still under investigation. The breakdown of the Poynting vector estimation procedure may be attributed to either $\mu_1 = e^{j\frac{2\pi}{\lambda}\Delta u_1}$ and $\mu_2 = e^{j\frac{2\pi}{\lambda}\Delta u_2}$ becoming nearly identical, or $\nu_1 = e^{j\frac{2\pi}{\lambda}\Delta v_1}$ and $\nu_2 = e^{j\frac{2\pi}{\lambda}\Delta v_2}$ becoming nearly identical, when $\Delta$ is near 32 wavelengths. The breakdown of the disambiguation procedure at and above $\Delta = 32\lambda$ may be attributed to picking the wrong grid value in a few of the 300 trial runs. It is well known that the sample variance and sample bias estimators employed in these simulations are not robust and are highly sensitive to a few outliers.

For purposes of comparison, simulations were conducted with an L-shaped array of 18 unpolarized scalar sensors, with 9 elements uniformly spaced at a half-wavelength along both the $x$ and $y$ axes. This results in an $18 \times 1$ array-manifold (same length as in the 3 vector sensor case) and an array aperture of roughly 8 half-wavelengths along either axis. Employing the same signal parameters presented previously, the unpolarized scalar sensor array yielded an RMS standard deviation of $5 \times 10^{-4}$ for source 1. The 3 vector sensor array and attendant algorithm achieved the same RMS standard deviation with $\Delta = 1.5\lambda$ (3 half-wavelengths,) *i.e.*, with less than half the aperture of the unpolarized L-shaped array! This performance gain is due to the polarization diversity inherent in a vector sensor array. The performance gain of the vector sensor array and attendant algorithm proposed in this paper relative to the L-shaped array with the same number of component antennas becomes even more dramatic as $\Delta$ is increased. Increasing the inter-element spacing in the latter case is not feasible since the ambiguities induced would not be resolvable.

## 5. CONCLUSION

A novel ESPRIT-based 2D angle estimation scheme was proposed involving the use of a right-triangular array of three vector sensors spaced much farther apart than a half-wavelength. Simulations were presented showing the exceptional estimation accuracy one can achieve with a large extended aperture allowed by the disambiguation facilitated by the electromagnetic field information provided by the vector sensors. Processing three vector sensors according to the method developed in this paper allows one to estimate the azimuth and elevation angle of up to a maximum of six sources. In order to handle more sources, the proposed scheme may be extended for a larger number of vector sensors spaced according to a rectangular array geometry with inter-vector spacings much greater than a half-wavelength. This will be presented in the journal version of the paper.

## 6. REFERENCES


[1] D. W. Swingler & R. S. Walker, "Line-Array Beamforming Using Linear Prediction for Aperture Interpolation and Extrapolation", *IEEE Trans. ASSP*, pp. 16-30, Jan. '89.

[2] A. Nehorai & E. Paldi, "Vector-Sensor Array Processing for Electro-magnetic Source Localization", *IEEE Trans. Signal Processing*, pp. 376-398, Feb. 1994.

[3] A. Paulraj, R. Roy & T. Kailath, "Estimation of Signal Parameters Via Rotational Invariance Techniques-ESPRIT", *Proc. 19th Asilomar Conf.*, 1985.

[4] A. J. van der Veen, P.B. Ober, & E. F. Deprettere,"Azimuth and Elevation Computation in High Resolution DOA Estimation", *IEEE Trans. Signal Processing*, pp. 1828-1832, July 1992.


Figure 1: RMS standard deviation of $\hat{u}_1$ and $\hat{v}_1$ vs. inter-vector sensor spacing.

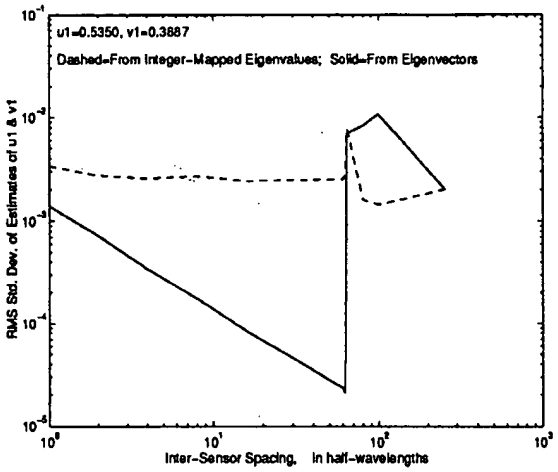


Figure 2: RMS bias of $\hat{u}_1$ and $\hat{v}_1$ vs. inter-sensor spacing.

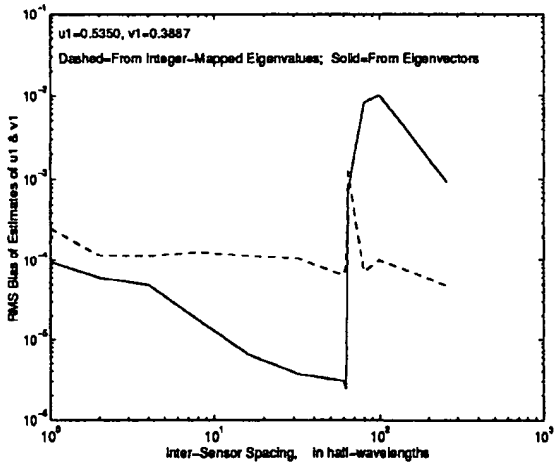

# DOA estimation for noninteger linear antenna arrays with more uncorrelated sources than sensors

Abramovich, Y.I. Spencer, N.K. Gorokhov, A.Y.
Cooperative Res. Centre for Sensor Signal & Inf. Process., Adeliade, SA;
*This paper appears in:* **Signal Processing, IEEE Transactions on**
On page(s): 943-955
Volume: 48, Issue: 4, Apr 2000
ISSN: 1053-587X
References Cited: 26
CODEN: ITPRED
INSPEC Accession Number: 6564079

**Abstract:**
We investigate direction-of-arrival (DOA) estimation involving nonuniform linear arrays, where the sensor positions may be noninteger values expressed in half-wavelength units, with some number of uncorrelated Gaussian sources that is greater than or equal to the number of sensors. We introduce an approach whereby the (noninteger) co-array is treated as the most appropriate virtual array when considering an augmented covariance matrix. Since such virtual arrays have an incomplete set of covariance lags, we discuss various completion philosophies to fill in the missing elements of the associated partially specified Hermitian covariance matrix. This process is followed by the application of an algorithm that searches for a specific number of plane wavefronts, yielding the minimum fitting error for the specified covariance lags in the neighborhood of the completion-initialized DOA estimates. In this way, we are able to resolve possible ambiguity and to achieve asymptotically optimal estimation accuracy. Numerical simulations of DOA estimation demonstrate a close proximity to the Cramer-Rao bound

**Index Terms:**
antenna theory array signal processing covariance matrices direction-of-arrival estimation linear antenna arrays Cramer-Rao bound DOA estimation augmented covariance matrix completion-initialized DOA estimates covariance lags direction-of-arrival minimum fitting error noninteger co-array noninteger linear antenna arrays nonuniform linear arrays partially specified Hermitian covariance matrix plane wavefronts sensor positions sensors uncorrelated Gaussian sources uncorrelated sources virtual array



**Reference list:**

1, J.-J. Fuchs, " Extension of the Pisarenko method to sparse linear arrays", *Proc. Int. Conf. Acoust., Speech Signal Process.*, Detroit, MI, pp.2100-2103, 1995.
[Abstract] [PDF Full-Text (392KB)]

2, K. Sharman, "Maximum likelihood parameter estimation by simulated annealing", *Proc. Int. Conf. Acoust., Speech Signal Process.*, New York, pp.2741-2744, 1988.

# DOA Estimation for Noninteger Linear Antenna Arrays with More Uncorrelated Sources than Sensors

Yuri I. Abramovich, *Member, IEEE*, Nicholas K. Spencer, and Alexei Y. Gorokhov, *Member, IEEE*

***Abstract*—We investigate direction-of-arrival (DOA) estimation involving nonuniform linear arrays, where the sensor positions may be noninteger values expressed in half-wavelength units, with some number of uncorrelated Gaussian sources that is greater than or equal to the number of sensors. We introduce an approach whereby the (noninteger) co-array is treated as the most appropriate *virtual array* when considering an augmented covariance matrix. Since such virtual arrays have an incomplete set of covariance lags, we discuss various completion philosophies to fill in the missing elements of the associated partially specified Hermitian covariance matrix. This process is followed by the application of an algorithm that searches for a specific number of plane wavefronts, yielding the minimum fitting error for the specified covariance lags in the neighborhood of the completion-initialized DOA estimates. In this way, we are able to resolve possible ambiguity and to achieve asymptotically optimal estimation accuracy. Numerical simulations of DOA estimation demonstrate a close proximity to the Cramér–Rao bound.**

***Index Terms*—Antenna arrays, array signal processing, direction-of-arrival estimation, linear arrays, nonuniformly spaced arrays.**

## I. Introduction

Consider an $M$-element noninteger-spaced nonuniform linear array, where the sensor positions may be noninteger values (measured in half-wavelength units). Since such an array generates up to $\frac{1}{2}M(M-1)$ distinct nonzero covariance lags, it has the potential [1] to estimate a *superior* number of uncorrelated sources $m$, meaning that this number is greater than or equal to the number of antenna elements

$$M \leq m \leq \tfrac{1}{2}M(M-1). \tag{1}$$

The only currently existing techniques that may be applied to the superior case for such arrays are the multidimensional maximum-likelihood search [2] and the geometry-invariant model-fitting idea [1], [3].

Here, we further investigate the geometry-based generalized augmentation approach (GAA) [4] and develop it for superior scenarios and noninteger linear arrays. We restrict our investigation to the case of *uncorrelated* Gaussian sources. Clearly, a large class of practical problems is excluded by this assumption. However, some modeling restrictions are necessary to achieve superior-scenario capabilities.

Another type of imposed restriction occurs for the existing high-order-moment algorithms [5], where the assumption of independency and non-Gaussianity is essential in achieving "blind" separation of such sources. It seems quite natural that although a *conventional* number of sources (defined as $1 \leq m < M$) can be localized, e.g., by MUSIC, under quite mild conditions, every attempt to extend localization capabilities beyond this limit involves some additional restrictions.

The overall idea behind our approach is to use the noninteger co-array as the virtual array. Since the original set of specified (measurable) covariance lags is incomplete for this choice of virtual array, the DOA (spatial spectrum) estimation problem can be formulated in terms of a positive-definite (p.d.) Hermitian completion problem, analogously to the p.d. Toeplitz completion problem for partially augmentable (integer) arrays [6]. Among possible completion criteria, we first investigate maximum-entropy (ME) completion and explore the limitations of this approach. For the special class of noninteger arrays that are slight perturbations (in terms of antenna locations) of fully augmentable arrays, we introduce a better "minimum-deflective" completion.

Since the proposed virtual array of co-array geometry is itself nonuniform, even with perfect completion, such an array can still suffer from *manifold ambiguity* [7]–[9]. Under our signal model, this means that for some particular scenarios, the co-array manifold (steering) vectors are linearly dependent. Therefore, MUSIC-type algorithms applied even to these perfectly completed covariance matrices will yield a set of ambiguous DOA estimates.

Our goal in this paper is to find some technique of properly identifying the true sources for superior scenarios, provided that they are potentially *identifiable*. For a conventional number of (independent) sources, this question was addressed in [9]. Here, we extend that approach, whose main idea is to find the best single fit between the set of estimated covariance lags and the DOA and power estimates, using initial DOA estimates obtained by completion. In this way, we can determine those directions that actually correspond to the true signals, as opposed to those that have essentially zero power. Simultaneously, we are able to refine our DOA estimates to the asymptotically optimal benchmark defined by the Cramér–Rao bound (CRB).

We present results of numerical simulations that compare the actual accuracy achieved by our proposed algorithms against the CRB. For practical reasons, for any finite $N$ and, hence, finite covariance lag estimation accuracy, we are also interested what

Manuscript received January 15, 1997; revised October 6, 1999. This work was supported in part by a grant from INTAS SASPARC. Some results of this paper were presented at the ICASSP Conference, Munich, Germany, 1997. The associate editor coordinating the review of this paper and approving it for publication was Editor-in-Chief José M. F. Moura.

Y. I. Abramovich and N. K. Spencer are with the Cooperative Research Centre for Sensor Signal and Information Processing (CSSIP), Adelaide, Australia.

A. Y. Gorokhov is with the Laboratoire des Signaux et Systèmes, École Supérieure d'Electricité, Paris, France.

Publisher Item Identifier S 1053-587X(00)02378-3.

level of intersource correlation can be tolerated by our methods without a significant loss in DOA estimation accuracy. Correspondingly, the robustness of our basic assumption regarding source independency will be analyzed in a quantitative manner.

This paper addresses the above-mentioned issues with the following structure. Background material is summarized in Section II. In Section III, we introduce our technique for ME p.d. completion. Section IV describes our "minimum-deflective" completion as an alternative to ME completion. Section V is devoted to manifold ambiguity resolution and local DOA estimation refinement, as well as the nonidentifiability conditions that preclude such resolution by any means. Section VI presents the results of numerical simulations in comparison with the CRB, whereas Section VII summarizes the paper.

## II. Background

Consider $m$ narrowband planewave signals of power $\boldsymbol{p} \equiv [p_1, \cdots, p_m]$ impinging on a nonuniform linear array of $M$ identical omnidirectional sensors located at positions $\boldsymbol{d} \equiv [0, d_2, \cdots, d_M]$ measured in half-wavelength units. We assume that the number of plane-wave sources $m$ is known. Adopting the commonly used data model [10], we have

$$\boldsymbol{y}(t) = S(\boldsymbol{\theta})\,\boldsymbol{x}(t) + \boldsymbol{\eta}(t), \quad \text{for } t = 1, \cdots, N \tag{2}$$

where

$$\begin{aligned} &\boldsymbol{x}(t) = [x_1(t), \cdots, x_m(t)]^T, \quad \boldsymbol{y}(t) = [y_1(t), \cdots, y_M(t)]^T \\ &\boldsymbol{\eta}(t) = [\eta_1(t), \cdots, \eta_M(t)]^T \end{aligned} \tag{3}$$

$x_j(t)$ $(j = 1, \cdots, m)$ is the complex signal amplitude of the $j$th plane wave, and where $y_k(t)$ and $\eta_k(t)$ $(k = 1, \cdots, M)$ are the sensor output and the noise at the $k$th sensor, respectively. To permit DOA estimation in the superior case $(m \geq M)$, we restrict ourselves to the class of independent Gaussian signal amplitudes $\boldsymbol{x}(t) \in C^{m\times 1}$ such that

$$\mathcal{E}\{\boldsymbol{x}(t_1)\boldsymbol{x}^H(t_2)\} = \begin{cases} P \equiv \text{diag}[\boldsymbol{p}], & \text{for } t_1 = t_2 \\ 0, & \text{for } t_1 \neq t_2. \end{cases} \tag{4}$$

We assume that the additive noise $\boldsymbol{\eta}(t) \in C^{M\times 1}$ is white and Gaussian

$$\mathcal{E}\{\boldsymbol{\eta}(t_1)\boldsymbol{\eta}^H(t_2)\} = \begin{cases} p_0 I_M, & \text{for } t_1 = t_2 \\ 0, & \text{for } t_1 \neq t_2. \end{cases} \tag{5}$$

The array manifold matrix is $S(\boldsymbol{\theta}) \equiv [\boldsymbol{s}(\theta_1), \cdots, \boldsymbol{s}(\theta_m)] \in C^{M\times m}$, where each constituent "steering vector" $\boldsymbol{s}(\theta_k)$ is defined as

$$\boldsymbol{s}(\theta_j) = [1, \exp(i\pi d_2 w_j), \cdots, \exp(i\pi d_M w_j)]^T \tag{6}$$

with $\boldsymbol{w} = \sin\boldsymbol{\theta} \in [-1, 1]$.

According to this model, the $M$-variate spatial covariance matrix

$$R = SPS^H + p_0 I_M \tag{7}$$

is p.d. Hermitian. Note that in our case of $m \geq M$, the noise-free covariance matrix $SPS^H$ is generally of full rank. Given $N$ independent samples ("snapshots"), the sufficient statistic for DOA estimation is the $M$-variate direct data covariance (DDC) matrix

$$\hat{R} = \frac{1}{N}\sum_{t=1}^{N} \boldsymbol{y}(t)\boldsymbol{y}^H(t). \tag{8}$$

Under our assumptions, $\hat{R}$ is characterized by a complex Wishart distribution $N\hat{R} \sim \mathcal{CW}(N, M, R)$, nondegenerate for $N \geq M$, and thus, the CRB can be readily calculated [10] to provide the asymptotic bound on DOA estimation accuracy for every "locally identifiable" scenario (i.e. with nondegenerate Fisher information matrix) [9]. We use the CRB as our DOA estimation accuracy benchmark.

To illustrate the problems that arise in the superior case, consider the four-element noninteger array introduced by Proukakis and Manikas [7]

$$\boldsymbol{d}_1 = [0, 1.2, 3.4, 4.6]. \tag{9}$$

In considering the superior scenario, we begin with the observation that the co-array of $\boldsymbol{d}_1$ is $\boldsymbol{c}_1 = [0, 1.2, 2.2, 3.4, 4.6]$, i.e., this geometry specifies the set of $L = 5$ covariance lags

$$\begin{aligned} \boldsymbol{r} &\equiv [r_j]_{j\in\mathcal{D}} \equiv [r_{(c_j)}]_{j=1,\cdots,L} \\ &= [r_{(0)}, r_{(1.2)}, r_{(2.2)}, r_{(3.4)}, r_{(4.6)}] \end{aligned} \tag{10}$$

(where $L$ is the number of co-array elements and, of course, is equivalent here to $M_\alpha$), which is the number of virtual array sensors, which means that the maximum number of potentially identifiable sources in this case is $m_{\max} = 4$, whereas the number of (real) degrees of freedom is $2L - 1 = 9$ [1]. In addition, note that the co-array geometry $\boldsymbol{c}_1$ still meets the sufficient condition for manifold ambiguity defined in [7]

$$c_L > L - 1. \tag{11}$$

The Proukakis–Manikas technique for determining ambiguity generator sets (AGS's) may be applied to the co-array to find that there is a single AGS associated with $\boldsymbol{c}_1$, which is

$$\boldsymbol{w}_{AGS} = [-0.8391, -0.4043, 0.0304, 0.4652, 0.9]. \tag{12}$$

Thus, for the (virtual) array $\boldsymbol{c}_1$, any four DOA's from the set $\boldsymbol{w}_{AGS}$ result in all five MUSIC peaks, even if the true five-variate covariance matrix is used. While the array $\boldsymbol{d}_1$ and its co-array $\boldsymbol{c}_1$ share the same AGS $\boldsymbol{w}_{AGS}$, there is an important distinction; the ambiguity rank is equal to three for the array and four for the co-array. This means that any three manifoldly ambiguous independent sources obtained via the Proukakis–Manikas technique are identifiable for $\boldsymbol{d}_1$.

For the superior case of four sources with $\boldsymbol{d}_1$, we have to first devise a new DOA estimation approach, given the set of covariance lag estimates $\hat{\boldsymbol{r}}$, and, second, to explore avenues of ambiguity resolution given a manifoldly ambiguous scenario such as

$$\boldsymbol{w}_4 = [-0.8391, -0.4043, 0.0304, 0.4652]. \tag{13}$$

These two problems can be tackled independently since if the full set of ambiguous DOA's (five in this case) is somehow identified, all that remains is to decide which of them are true and

which are spurious. For an identifiable scenario, the manifold ambiguity resolution problem will have a unique solution.

In the next section, we discuss an approach capable of (possibly ambiguous) DOA estimation for a superior number of uncorrelated sources. We deal with manifold ambiguity resolution in Section V.

## III. Maximum-Entropy Positive-Definite Hermitian Completion

When the co-array $\boldsymbol{c}$ is selected as the virtual array, the set of specified covariance lags $\boldsymbol{r}$ defined by the array $\boldsymbol{d}$ is incomplete for the virtual array, as is the $L$-variate augmented Hermitian covariance matrix $H$. For our example noninteger geometry $\boldsymbol{d}_1 = [0, 1.2, 3.4, 4.6]$, the partially specified five-variate augmented covariance matrix is

$$H = \begin{bmatrix} r_{(0)} & r_{(1.2)} & r_{(2.2)} & r_{(3.4)} & r_{(4.6)} \\ r^*_{(1.2)} & r_{(0)} & ? & r_{(2.2)} & r_{(3.4)} \\ r^*_{(2.2)} & ? & r_{(0)} & r_{(1.2)} & ? \\ r^*_{(3.4)} & r^*_{(2.2)} & r^*_{(1.2)} & r_{(0)} & r_{(1.2)} \\ r^*_{(4.6)} & r^*_{(3.4)} & ? & r^*_{(1.2)} & r_{(0)} \end{bmatrix} \tag{14}$$

since the covariance lags $H_{2,3} \equiv r_{(1.0)}$ and $H_{3,5} \equiv r_{(2.4)}$ are not presented by the array $\boldsymbol{d}_1$. Thus, DOA estimation for noninteger NLA's is closely connected with the mathematical completion problem for partially specified Hermitian matrices. Since maximum likelihood (ML) completion is not directly attainable, we will instead propose some other *ad hoc* completion, followed by ML refinement.

We begin with maximum-entropy (ME) completion, although, in general, as a result of ME completion, we may obtain a solution that cannot possibly correspond to a plane-wave model. Moreover, since entropy is defined by the determinant of the covariance matrix for a Gaussian process, ME completion may significantly increase the effective signal subspace, i.e., the number of eigenvalues significantly greater than the white noise power $p_0$ or, on the contrary, may increase the virtual "noise floor" in the completed matrix. This is why we have to be cautious applying ME completion, and we should be prepared to treat it only as an initial step.

Let the general virtual array $\boldsymbol{d}'$ be specified by the virtual sensor positions $d'_j$ $(j = 1, \cdots, M')$; then, the set of all possible p.d. Hermitian completions $\mathcal{H}$ may be written as

$$\mathcal{H} = \left\{ z\colon H(z) = H_0 + \sum_{\substack{p,q \in \overline{\mathcal{S}} \\ p<q}} (\operatorname{Re} H_{pq} E^{pq}_{+} + i \operatorname{Im} H_{pq} E^{pq}_{-}) > 0 \right\} \tag{15}$$

where

$$z = \begin{bmatrix} \operatorname{Re} H_{pq} \\ \operatorname{Im} H_{pq} \end{bmatrix}_{pq \in \overline{\mathcal{S}} p<q}, \quad E^{pq}_{+} = e_p e_q^T + e_q e_p^T$$
$$E^{pq}_{-} = e_p e_q^T - e_q e_p^T \tag{16}$$

and where $e_p = [0, \cdots, 0, 1, 0, \cdots, 0]$ is the $M'$-variate basis vector with a unit entry in the $p$th position, $H_0$ is the augmented covariance matrix with zeros in place of the unspecified elements of $H$, $\mathcal{S}$ is the set of specified elements $\{p, q\}$ of $H$, and $\overline{\mathcal{S}}$ is the set of unspecified elements in the initial incomplete augmented covariance matrix $H$. The specified elements of $H$ are defined by the standard direct augmentation approach (DAA) [11] operating on the $M$-variate covariance matrix $R$ (7)

$$H_{pq \in \mathcal{S}} = \frac{\sum_{j,k=1}^{M} R_{jk} \delta(v_p - v_q, d_j - d_k)}{\sum_{j,k=1}^{M} \delta(v_p - v_q, d_j - d_k)}. \tag{17}$$

In practical situations, we apply the DAA to the DDC matrix $\hat{R}$ (8) to obtain $\hat{H}$.

Suppose we label each of the missing lags ($pq \in \overline{\mathcal{S}}; p < q$) from 1 to $\ell$, which is the total number of missing lags. In our example, we then have the set of $\ell = 2$ missing lags $\overline{\mathcal{S}} = \{H_{2,3} \equiv r_{(1.0)}, H_{3,5} \equiv r_{(2.4)}\}$. Then, we may introduce the following notation instead of (15):

$$\mathcal{H} = \left\{ z\colon H(z) = H_0 + \sum_{j=1}^{2\ell} z_j F_j > 0 \right\} \tag{18}$$

where

$$z_j = \begin{cases} \operatorname{Re} r_{pq \in \overline{\mathcal{S}}; p<q}, & \text{for } j = 1, \cdots, \ell \\ \operatorname{Im} r_{pq \in \overline{\mathcal{S}}; p<q}, & \text{for } j = \ell+1, \cdots, 2\ell \end{cases}$$
$$F_j = \begin{cases} E^{pq}_{+}, & \text{for } j = 1, \cdots, \ell \\ i E^{pq}_{-} & \text{for } j = \ell+1, \cdots, 2\ell. \end{cases} \tag{19}$$

Let us assume for the moment that the feasibility condition for the p.d. completion of $H(z)$ is satisfied, i.e., there exists at least one solution $z$ for the *linear matrix inequality* (LMI) [12] $H(z) > 0$. For exact covariance lags (deterministic completion), this is always true since there exists the p.d. completion corresponding to the true DOA's and the virtual array. When the feasibility condition is guaranteed, the following theorem may be immediately applied.

*Theorem 1:* [13], [14] Let $H$ be a partially specified positive-definite matrix, all of whose diagonal elements are specified, and suppose that $H$ admits at least one positive-definite completion. Then, among all such completions, there is a unique one with maximum determinant. Furthermore, this determinant-maximizing positive-definite completion $H_{ME}$ is characterized by having a zero in its inverse in every position where $H$ has an unspecified element.

This theorem generalizes the well-known property of the Burg ME spectrum, whereby an ME-extended Toeplitz covariance matrix has zeroes in its inverse for every unspecified subdiagonal (the auto-regressive property) [15].

According to Theorem 1, the function

$$\phi(z) = \begin{cases} \log \det H^{-1}(z), & \text{for } z \in \mathcal{H} \\ \infty, & \text{otherwise} \end{cases} \tag{20}$$

is strictly convex on the feasible set and therefore has the unique minimizer

$$z_{ME} = \arg \min_{\mathcal{H}} \phi(z) = \arg \max_{\mathcal{H}} \det H(z) \tag{21}$$

which is called the *analytic center* of the LMI $H(z) > 0$. For Gaussian distributions, we may evidently treat the analytic center as the ME completion since the entropy for Gaussian-distributed random variables of zero mean is given by [15] $E = \frac{1}{2}\log(\det H)$, where $H$ is the correlation matrix.

Let us now turn to the problem of computing the analytic center of the LMI. Since the feasibility conditions are assumed to hold at this stage, the search for the analytical center can be split into two subproblems. First, define an arbitrary feasible point $\check{z}$ such that $H(\check{z}) > 0$. Second, given $\check{z}$, any convergent procedure that minimizes $\phi(z)$ (taking into account the feasibility condition) will converge to the analytical center $z_{ME}$. For details of the Ellipsoid and Newton algorithms used to solve these two convex programming problems, see [12] and [16], but to summarize, convex programming solves the generalized problem of finding the ME completion for an arbitrary feasible incomplete covariance matrix.

When the sufficient statistic is provided in the form of a $M$-variate sample covariance matrix $\hat{R}$ characterized by a complex Wishart distribution $\mathcal{CW}(N, M, R)$, the set of sample specified covariance lags $\hat{r}$ is usually obtained via the direct augmentation approach of (17) with sample covariance lags instead of exact values. In this case, the feasibility condition for the existence of a p.d. Hermitian completion is no longer guaranteed to hold.

The question of which partially specified Hermitian matrices may be p.d. completed is addressed in [14]. It was shown that if the diagonal elements are specified, if the principal minors of the specified elements are positive, and if the undirected graph of the specified elements is chordal, then a p.d. completion exists. This last condition always seems to be satisfied for the augmentation approach simply because the p.d. completion always exists for the exact covariance lags (with the same undirected graph, of course). Instead of forming all principal minors, we may simply associate the success of the Ellipsoid Algorithm in finding a feasible point $\check{z}$ with the feasibility condition mentioned above.

Hence, if the necessary and sufficient condition fails (the feasible point $\check{z}$ is not achievable by the Ellipsoid Algorithm), we need to modify the set of sample specified covariance lags in order to achieve feasibility with the minimum possible deflection from the initial set of (maximum likelihood) estimates $\hat{r}$. Several approaches for such a modification may be proposed. For example, by introducing

$$\hat{H}(z) = \hat{H}_0 + \sum_{j\in\mathcal{S}} z_j' F_j + \sum_{j\in\overline{\mathcal{S}}} z_j F_j \tag{22}$$

similarly to (18), we may find the minimum-deflective point by the solution of the optimization problem

$$\text{find } \min \sum_{j\in\mathcal{S}} (z_j')^2 \quad \text{subject to } \hat{H}(z) > 0. \tag{23}$$

The Ellipsoid Algorithm provides a straightforward approach to find the unique optimum solution.

Another possibility is to define the minimal diagonal loading for the matrix $\hat{H}(z)$ to achieve feasibility, which is also a standard convex optimization problem. In general, all these approaches may provide different solutions in particular cases. Nevertheless, we do not expect statistically different results in the asymptotic domain, where in accordance with the Cramér–Rao bounds, we expect reasonable convergence to the true DOA's.

We note that this ME Hermitian completion approach is valid for arbitrary-geometry arrays, e.g., 2-D.

## IV. ME and MD Positive-Definite Hermitian Completion

The noninteger NLA $\boldsymbol{d}_1 = [0, 1.2, 3.4, 4.6]$ introduced by Proukakis and Manikas [7] is an example of a poor geometry choice for DOA estimation purposes since it has only five distinct covariance lags rather than the maximum possible of $\frac{1}{2}M(M-1)+1 = 7$. In order to increase the number of potentially identifiable sources, all redundancies should be avoided.

Let us instead turn our attention to the noninteger array

$$\boldsymbol{d}_2 = [0, 1.09, 3.96, 5.93] \tag{24}$$

which is recognizable as a slightly perturbed version of the "optimal-lag" (nonredundant *and* fully augmentable) integer array $d = [0, 1, 4, 6]$ investigated by Moffet [17]. In practical applications, such geometry perturbations are usually caused by antenna positioning errors. This *quasi-fully augmentable* array $\boldsymbol{d}_2$ is also nonredundant and generates the full set of seven lags:

$$\boldsymbol{c}_2 = [0, 1.09, 1.97, 2.87, 3.96, 4.84, 5.93]. \tag{25}$$

Naturally, this co-array is a slightly perturbed version of the seven-element ULA. In this case, the array manifold ambiguity condition $d_M > M-1$ is satisfied, whereas the co-array manifold ambiguity condition $c_L > L-1$ is not satisfied, and therefore, the only currently existing method (the Proukakis–Manikas technique) is unable to find any AGS's for the co-array $\boldsymbol{c}_2$.

The class of noninteger linear arrays that do not satisfy the co-array manifold ambiguity condition may be called *GIMP identifiable* since, like fully augmentable (integer) arrays, their co-arrays appear to have no AGS's, and therefore, they would be *globally* identifiable (identifiable regardless of the DOA set). We have conditioned this assertion by the acronym GIMP for two reasons. First, because this is true assuming Gaussian independent sources, and second, because the Proukakis–Manikas technique does not yet guarantee to produce an exhaustive list of AGS's, i.e., the manifold ambiguity condition $d_M > M-1$ has been proven to be sufficient, but it is not known whether it is necessary.

While the potential capabilities of the array $\boldsymbol{d}_2$ are obviously more attractive than those of $\boldsymbol{d}_1$, the problem of $L$-variate augmented covariance matrix completion is slightly different in this case. Nonredundant arrays have the number of co-array elements $L = \frac{1}{2}M(M-1)+1$, whereas the number of unspecified covariance lags in the $L$-variate augmented covariance matrix is $\ell = \frac{1}{2}(L-1)(L-2)$. Even prior to computational examples, we may expect for $M \gg 1$ that the extreme incompleteness of the augmented matrix might lead to an ME completion that is quite inconsistent with the DOA estimation problem. In fact, the inverse of the ME completion ($H_{ME}^{-1}$) will have exactly $\ell$ zeroes

in the position of each missing lag and is obviously radically different from the structure of the inverse of the true covariance matrix $H_{exact}^{-1}$ for $m$ independent plane waves.

In view of these misgivings regarding the appropriateness of the ME completion, it seems quite natural to exploit the close proximity of the perturbed array geometry to the corresponding integer array. In the case of quasifully augmentable arrays, the following *minimum-deflective* (MD) completion treats the true Hermitian matrix $H_{exact}$ as a slightly perturbed Toeplitz matrix. We can write each missing lag of the augmented Hermitian matrix as a perturbation such as

$$H_{pq} = H_{jk} + z_n + iz_{n+\ell} \quad \text{for } n, p, q \in \overline{\mathcal{S}}; \quad j, k \in \mathcal{S} \tag{26}$$

where the nearest specified covariance lag is used

$$\min_{jk} \Big| \, |c_j - c_k| - |c_p - c_q| \, \Big|. \tag{27}$$

In fact, the same approximation may be made for any type of noninteger array, such as $\boldsymbol{d}_1$, where

$$H_{2,3} \equiv r_{(1.0)} = r_{(1.2)} + z_1 + iz_2 \tag{28}$$

$$H_{3,5} \equiv r_{(2.4)} = r_{(2.2)} + z_3 + iz_4. \tag{29}$$

In general, within the set of specified covariance lags $\mathcal{S}$, we can always find the "nearest" existing lag to any given missing lag of the virtual array (the co-array) and use this completion $H_T$ instead of $H_0$. Naturally, this completion may not be a feasible covariance matrix since this process cannot guarantee the positive-definiteness of $H_T$.

The definition of the minimum-deflective solution $\boldsymbol{z}_{MD}$ that makes the $L$-variate Hermitian matrix $H(\boldsymbol{z}_{MD}) \equiv H_{MD}$ nonnegative definite is

$$\text{find} \quad \min \sum_{j \in \overline{\mathcal{S}}} |z_j|^2 \quad \text{subject to}$$

$$H(\boldsymbol{z}) = H_T + \sum_{j=1}^{2\ell} z_j F_j \geq 0. \tag{30}$$

For our example array, $\boldsymbol{d}_2$, $\ell = \frac{1}{2}(L-1)(L-2) = 15$.

It is now clear that we may treat this MD completion as a Pisarenko-type completion [6]. Formally, the problem (30) is identical to the minimum-deflective initial point search with the initial matrix $H_0$ replaced by $H_T$. We may make such a completion more effective by modifying the diagonal element by a fixed correction in noise power $(\hat{r}_0 - p_0)$, or by an optimised deflection $(\hat{r}_0 - \lambda)$, provided that the feasibility condition is not violated.

To summarize, convex programming techniques provide computationally effective completions of partially specified Hermitian covariance matrices of the so-called virtual array that may be used to initialise DOA estimation.

## V. Manifold Ambiguity Resolution and Local DOA Refinement

There are four major reasons why DOA estimates obtained by the above completion methods need to be refined. First, we have shown that the virtual array can suffer from manifold ambiguity, even for the true (deterministic) $L$-variate covariance matrix. Second, even for the true covariance lags $\boldsymbol{r}$ specified by $\boldsymbol{d}$, the ME- and MD-completion techniques do not necessarily yield the true DOA estimates, i.e., these techniques lead to biased estimates. Third, ME completion increases the determinant of the completed matrix $H$; in turn, this has the potential to introduce spurious sources. This "self-induced" ambiguity is a more serious problem than co-array manifold ambiguity since the latter exists only for very specific DOA sets (defined by the AGS's), whereas the former phenomenon can arise in an arbitrary DOA scenario.

The final reason is that the DAA adopted for estimating specified covariance lags has been proven to be far from asymptotically optimal [11], even in its pure form. Naturally, the result of the additional step of completing a partially specified matrix cannot *generally* improve the overall DAA performance. This qualification is important since the biased nature of DOA estimates obtained via completion may, in principle, lead to *super-efficient* estimates [18] in particular cases.

Given the set of initial DOA estimates obtained by a completion method, we next have to solve two problems. First, we need to be able to resolve either (or both) of the ambiguity types mentioned above (co-array manifold ambiguity and self-induced ambiguity). Second, having eliminated the spurious DOA estimates, we need to increase the accuracy of the properly identified estimates in order to reduce any bias introduced by completion and to reduce the stochastic estimation errors as close as possible to the CRB limit. By assuming in this paper that the CRB is finite, we are deliberately excluding situations where the Fisher information matrix is degenerate, i.e., where the scenario is *locally nonidentifiable* [9].

### A. Manifold Ambiguity versus Nonidentifiability

Here, we consider the problem of determining whether any manifoldly ambiguous scenario (with independent Gaussian sources) is, in fact, nonidentifiable. We will shortly see that the approach presented here is also capable of resolving the "self-induced" ambiguity created by ME completion.

According to the model described by (4) and (7), the set of specified spatial covariance lags may be presented in the form

$$\boldsymbol{r}' = A(\boldsymbol{\theta})\boldsymbol{p} \quad \text{for } \boldsymbol{p} > 0 \tag{31}$$

where $\boldsymbol{r}' = [r_0 - p_0, r_1, \cdots, r_{L-1}]^T$ is the white-noise modified $L$-variate vector of specified covariance lags, and $A(\boldsymbol{\theta}) \equiv [\boldsymbol{a}(\theta_1), \cdots, \boldsymbol{a}(\theta_m)]$ is the $L \times m$ co-array manifold matrix, with

$$\boldsymbol{a}(\theta_j) = [1, \exp(i\pi c_2 w_j), \cdots, \exp(i\pi c_L w_j)]^T. \tag{32}$$

*Pointwise nonidentifiability* therefore occurs at the point $\boldsymbol{\theta}_*$ if there exists a different set of $m$ DOA's $\boldsymbol{\theta}'_* \neq \boldsymbol{\theta}_*$ and two sets of (possibly different) non-negative powers $\boldsymbol{p}_*, \boldsymbol{p}'_*$ such that

$$A(\boldsymbol{\theta}_*)\boldsymbol{p}_* = A(\boldsymbol{\theta}'_*)\boldsymbol{p}'_*. \tag{33}$$

Obviously, this will occur when there exist the pairs $\boldsymbol{\theta}'_* \neq \boldsymbol{\theta}_*$ and $\boldsymbol{p}_*, \boldsymbol{p}'_*$ such that their corresponding multivariate distributions are identical, i.e.,

$$f(\boldsymbol{y}|\boldsymbol{\theta}_*, \boldsymbol{p}_*) = f(\boldsymbol{y}|\boldsymbol{\theta}'_*, \boldsymbol{p}'_*) \tag{34}$$

since

$$R(\boldsymbol{\theta}_*, \boldsymbol{p}_*) = R(\boldsymbol{\theta}'_*, \boldsymbol{p}'_*). \tag{35}$$

Hence, (33), which is identical to (35) here, is the necessary and sufficient condition for nonidentifiability.

Note that we are discussing the case where the pair $\boldsymbol{\theta}'_*, \boldsymbol{\theta}_*$ may be chosen from a set of measure zero, where the Kullback directed divergence (KDD) $I(\boldsymbol{\theta}'_*, \boldsymbol{\theta}_*)$ between the corresponding Gaussian probability densities is strictly equal to zero [19], [20], and where the "generalized ambiguity" [20] is strictly equal to one.

Let us illustrate the distinction between the co-array manifold ambiguity condition (11) and the nonidentifiability condition (33) starting from the simple case when the set $\boldsymbol{\theta}'_*$ differs from $\boldsymbol{\theta}_*$ by a single DOA so that the set $\tilde{\boldsymbol{\theta}}_* = \boldsymbol{\theta}_* \cup \boldsymbol{\theta}'_*$ consists of $(m+1)$ DOA's. In this case, the necessary and sufficient condition for nonidentifiability (33) may be rewritten as

$$A(\tilde{\boldsymbol{\theta}}_*)\boldsymbol{h} = 0 \tag{36}$$

where

$$\boldsymbol{h} = \begin{bmatrix} p_{*1} \\ p_{*2} - p'_{*1} \\ \vdots \\ p_{*m} - p'_{*m-1} \\ -p'_{*m} \end{bmatrix} \tag{37}$$

with $\boldsymbol{p}_*, \boldsymbol{p}'_* > 0$. This condition can be rephrased as occurring when *the complex homogeneous linear system (36) admits a solution $\boldsymbol{h}$ that is real and has the property*

$$h_1 h_{m+1} < 0. \tag{38}$$

It is now clear that our application of the manifold ambiguity condition [7] to the co-array

$$\text{rank } A(\tilde{\boldsymbol{\theta}}_*) \leq m \tag{39}$$

that ensures the existence of an arbitrary nontrivial complex solution to (36) is only a *necessary* condition for nonidentifiability since it does not guarantee the extra two properties of $\boldsymbol{h}$. Thus, the Proukakis–Manikas technique applied to the co-array will generate only *potentially* nonidentifiable scenarios.

Since the solution $\boldsymbol{h}$ is required to be real, (36) can be rewritten as

$$\mathcal{A}(\tilde{\boldsymbol{\theta}}_*)\boldsymbol{h} = 0 \tag{40}$$

where

$$\mathcal{A}(\tilde{\boldsymbol{\theta}}_*) = \begin{bmatrix} \text{Re } A(\tilde{\boldsymbol{\theta}}_*) \\ \text{Im } A(\tilde{\boldsymbol{\theta}}_*) \end{bmatrix} \in \mathcal{R}^{(2L-1)\times(m+1)} \tag{41}$$

(the first row of the imaginary part is dropped since it is trivially equal to zero). An arbitrary nontrivial real solution of the new system (40) exists if and only if

$$\text{rank } \mathcal{A}(\tilde{\boldsymbol{\theta}}_*) \leq m. \tag{42}$$

This condition is clearly more stringent than (39); in fact, all AGS's generated for the co-array geometry examples mentioned below did not meet condition (42), whereas obviously, they did satisfy (39). Hence, (42) can be considered to be an additional necessary condition for nonidentifiability, and the list of co-array manifoldly ambiguous scenarios generated by the Proukakis–Manikas method may now be checked against (42) to further select potentially nonidentifiable scenarios.

Suppose that $\mathcal{A}(\tilde{\boldsymbol{\theta}}_*)$ is $\kappa$-rank-deficient, i.e., rank $\mathcal{A}(\tilde{\boldsymbol{\theta}}_*) = (m+1) - \kappa$, with $\kappa \geq 1$, so that every possible (real) solution to (40) can be written as

$$\boldsymbol{h} = \Phi \boldsymbol{x} \tag{43}$$

where $\Phi \in \mathcal{R}^{(m+1)\times\kappa}$ is the fundamental solution to the system (40), and $\boldsymbol{x} \in \mathcal{R}^{\kappa\times 1}$. The purpose of this step is to allow us to search for a possible solution $\boldsymbol{h}$ of (40) with the two extra constraints by formulating a linear programming (LP) problem. Using a standard "trick," we present the arbitrary real vector $\boldsymbol{x}$ in the form $\boldsymbol{x} = \boldsymbol{x}_1 - \boldsymbol{x}_2$ for some $\boldsymbol{x}_1, \boldsymbol{x}_2 \in \mathcal{R}_+^{\kappa\times 1}$ (i.e. positive-valued vectors). We can now verify that the following LP problem is appropriate for solving $\Phi\boldsymbol{x} - \boldsymbol{h} = 0$ with $h_1 h_{m+1} < 0$

$$\text{Find } \min(\lambda_1 + \lambda_2) \quad \text{for } \Phi(\boldsymbol{x}_1 - \boldsymbol{x}_2) - \begin{bmatrix} 0 \\ -\boldsymbol{y}_1 \\ 0 \end{bmatrix} - \begin{bmatrix} 0 \\ \boldsymbol{y}_2 \\ 0 \end{bmatrix} - \begin{bmatrix} y_3 \\ 0 \\ -y_4 \end{bmatrix} - \begin{bmatrix} -\lambda_1 \\ 0 \\ \lambda_2 \end{bmatrix} = 0 \tag{44}$$

where $y_1, y_2 \in \mathcal{R}_+^{(m-2)\times 1}$ and $y_3, y_4, \lambda_1, \lambda_2 > 0$ since if and only if the minimum solution is precisely zero will the solution $\boldsymbol{h}$ be of the required structure, namely

$$\boldsymbol{h} \equiv \Phi\boldsymbol{x} \equiv \Phi(\boldsymbol{x}_1 - \boldsymbol{x}_2) = \begin{bmatrix} y_3 \\ \boldsymbol{y}_2 - \boldsymbol{y}_1 \\ -y_4 \end{bmatrix} \tag{45}$$

where all the $y$'s are positive valued. Note that this LP problem is guaranteed to have a solution since for nonzero $\lambda_1, \lambda_2$, we can always write $\Phi(\boldsymbol{x}_1 - \boldsymbol{x}_2) = \boldsymbol{z}_1 - \boldsymbol{z}_2$ for some $\boldsymbol{z}_1, \boldsymbol{z}_2 \in \mathcal{R}^{m\times 1}$.

To summarize, the existence of a zero solution to the LP problem (44) is the necessary and sufficient condition of nonidentifiability for the co-array manifoldly ambiguous scenario $\tilde{\boldsymbol{\theta}}_* = \boldsymbol{\theta}_* \cup \boldsymbol{\theta}'_*$.

Note that in this same situation but with the different *a priori* model where the powers $p_{*j}$ $(j = 1, \cdots, m)$ must be identical ($p_{*j} = \rho$ say), nonidentifiability occurs under the more stringent condition

$$h_1 + h_{m+1} = 0; \quad h_j = 0 \quad \text{for } j = 2, \cdots, m \tag{46}$$

since the solution could be normalized such that $h_1 = \rho > 0$. The significant difference between the two conditions (38) and (46) is due to the fact already discussed in [9], [21], [22]: that *identifiability conditions strongly depend on the statistical signal model and are not defined by the array geometry alone.*

Up to this point, we assumed that $\tilde{\boldsymbol{\theta}}_* = \boldsymbol{\theta}_* \cup \boldsymbol{\theta}'_*$ consisted of $(m+1)$ DOA's. In general, it will consist of $m+1 \leq \ell \leq 2m$ DOA's so that only $(2m-\ell)$ DOA's belong to $\boldsymbol{\theta}_* \cap \boldsymbol{\theta}'_*$. For the arbitrary power model, the rank-deficiency of $\mathcal{A}(\tilde{\boldsymbol{\theta}}_*)$, $\kappa$ may be greater than one:

$$\text{rank } \mathcal{A}(\tilde{\boldsymbol{\theta}}_*) = \ell - \kappa \tag{47}$$

for $1 \leq \kappa \leq \ell - 2$, whereas the general necessary and sufficient condition for nonidentifiability is

$$\Phi\boldsymbol{x} - \begin{bmatrix} \boldsymbol{p}_* \\ 0 \end{bmatrix} + \begin{bmatrix} 0 \\ \boldsymbol{p}'_* \end{bmatrix} = 0 \tag{48}$$

where $\Phi \in \mathcal{R}^{\ell\times\kappa}$ is the fundamental solution to the system (40), $\boldsymbol{x} \in \mathcal{R}^{\kappa\times 1}$, and $\boldsymbol{p}_*, \boldsymbol{p}'_* \in \mathcal{R}_+^{m\times 1}$. As before, the solution to (48)

may be found by solving the following linear programming (LP) problem:

$$\text{Find } \min \sum_{j=1}^{\ell-m} (\lambda_{1j}+\lambda_{2j}) \quad \text{for } \Phi(\boldsymbol{x}_1-\boldsymbol{x}_2) + \begin{bmatrix} 0 \\ \boldsymbol{y}_1 \\ 0 \end{bmatrix} - \begin{bmatrix} 0 \\ \boldsymbol{y}_2 \\ 0 \end{bmatrix} + \begin{bmatrix} -\boldsymbol{y}_3 \\ 0 \\ \boldsymbol{y}_4 \end{bmatrix} + \begin{bmatrix} \boldsymbol{\lambda}_1 \\ 0 \\ -\boldsymbol{\lambda}_2 \end{bmatrix} = 0 \quad (49)$$

where $\boldsymbol{x}_1, \boldsymbol{x}_2 \in \mathcal{R}_+^{\kappa\times 1}$, $\boldsymbol{y}_1, \boldsymbol{y}_2 \in \mathcal{R}_+^{(2m-\ell)\times 1}$, and $\boldsymbol{y}_3, \boldsymbol{y}_4$, $\boldsymbol{\lambda}_1, \boldsymbol{\lambda}_2 \in \mathcal{R}_+^{(\ell-m)\times 1}$. The nonidentifiability condition (40) is satisfied if this minimum is zero. Thus, for any locally identifiable scenario $\boldsymbol{\theta}_*$ with arbitrary powers $\boldsymbol{p}_*$ and rank-deficient matrix $\mathcal{A}(\tilde{\boldsymbol{\theta}}_*)$, *pointwise nonidentifiability occurs if and only if the solution of this LP problem is equal to zero.* In other words, the necessary and sufficient condition for a locally identifiable uncorrelated Gaussian superior scenario to be pointwise nonidentifiable is

$$\sum_{j=1}^{\ell-m} (\lambda_{1j}+\lambda_{2j}) = 0. \quad (50)$$

Any such scenario that does not meet this condition is pointwise identifiable.

Note that if we had a method for exhaustively listing all AGS's that satisfy (39) for a given co-array, then deciding *whether an array is always identifiable or not* would reduce to testing each AGS against the condition (42) and then the LP zero solution. We have already mentioned that the only existing technique for calculating AGS's [7] does not guarantee finding the full set of all possible AGS's. Since our study relies on this Proukakis–Manikas technique, complete identifiability of any given array can only be given in terms of the same (possible) subset of AGS's. However, any given array and DOA scenario can be easily tested. For example, the co-array geometry $\boldsymbol{c}_1$ results in the single AGS $\boldsymbol{w}_{AGS} \equiv \sin\boldsymbol{\theta}_*$ by the Proukakis–Manikas technique, but this fails even to meet the second necessary condition (42). This means that the four-source scenario $\boldsymbol{w}_4$ is globally identifiable, despite its co-array manifold ambiguity.

### *B. Co-Array Manifold Ambiguity Resolution and Local DOA Refinement*

Given any co-array manifoldly ambiguous (but identifiable) scenario, we now wish to find an algorithm that can identify the true $m$ DOA's $\boldsymbol{\theta}_*$ amongst the set of $\ell \geq m+1$ DOA's $\tilde{\boldsymbol{\theta}}_*$ provided (for example) by MUSIC applied to the properly completed augmented covariance matrix $H$.

Since, for identifiable scenarios, there is a unique solution to the equation $\boldsymbol{r}' = A(\boldsymbol{\theta}_*)\boldsymbol{p}_*$, a straightforward idea is to consider the equation $\boldsymbol{r}' = A(\tilde{\boldsymbol{\theta}}_*)\tilde{\boldsymbol{p}}_*$ and note that exactly $(\ell-m)$ components of the $\ell$-variate positive-valued vector $\tilde{\boldsymbol{p}}_*$ will be equal to zero. Naturally, in the practical case when $\hat{\boldsymbol{r}}'$ and $\hat{\tilde{\boldsymbol{\theta}}}_*$ are estimated quantities, we should search for the best fit over all $\ell$ elements of $\hat{\tilde{\boldsymbol{p}}}_*$ and associate the $m$ greatest values with the true source powers.

Instead of the least-squares optimization introduced in [23], we suggest that this "diagonal fit" problem (DFP) be solved directly by another LP

$$\text{Find } \min \boldsymbol{f}^T\boldsymbol{x} \quad \text{subject to} \quad \hat{A}_{LP}\boldsymbol{x} = \hat{\boldsymbol{r}}'_r \quad \text{and} \quad \boldsymbol{x} \in \mathcal{R}_+^{(\ell+4L-4)\times 1} \quad (51)$$

where

$$\hat{A}_{LP} = \left[\mathcal{A}(\hat{\tilde{\boldsymbol{\theta}}}_*) \,\middle|\, \begin{matrix} \boldsymbol{0}^T \\ I_{2(L-1)} \end{matrix} \,\middle|\, \begin{matrix} \boldsymbol{0}^T \\ -I_{2(L-1)} \end{matrix}\right] \in \mathcal{R}^{(2L-1)\times(\ell+4L-4)} \quad (52)$$

$$\hat{\boldsymbol{r}}'_r = \begin{bmatrix} \operatorname{Re}\hat{\boldsymbol{r}}' \\ \operatorname{Im}\hat{\boldsymbol{r}}' \end{bmatrix} \in \mathcal{R}^{(2L-1)\times 1} \quad (53)$$

$$\boldsymbol{f} = [\underbrace{0,\cdots,0}_{\ell} \,|\, \underbrace{1,\cdots,1}_{4L-4}]^T. \quad (54)$$

Both Im $A(\hat{\tilde{\boldsymbol{\theta}}}_*)$ and Im $\hat{\boldsymbol{r}}'$ consist of $(L-1)$ rows since we have deleted the row trivially equal to zero. Since the first $\ell$ elements of $\boldsymbol{x}$ correspond to the powers, as the number of snapshots $N$ (composing the DDC matrix $\hat{R}$) tends to infinity, precisely $\kappa$ of these elements will tend to zero, whereas the remaining $m$ of these elements approach the powers corresponding to the true DOA's. Thus, the solution of the DFP is obtained by choosing the $m$ greatest values amongst the first $\ell$ elements of $\boldsymbol{x}$.

This approach was inspired, in part, by Fuchs' model-fitting method [3], [24], as well as some of our early investigations into LP applications for array processing [25]. This basic LP problem (51)–(54) can be modified in different ways; for example, in addition to the mismatch minimization, we could also minimize the smallest element within the first $\ell$ elements of $\boldsymbol{x}$. It should be clear that the solution of the DFP does not depend on the array geometry and could be easily generalized for arbitrary nonlinear arrays (circular, 2-D, etc.), provided that identifiability is guaranteed for the given scenario.

For the superior case, where the DOA estimates are initialized by a completion technique, ambiguity resolution should be followed by some sort of ML refinement to achieve near asymptotic efficiency for the final DOA estimates. The algorithm shown at the bottom of the next page includes such a local refinement (at Step 5).

## VI. Simulation Results

To demonstrate the efficiency of the proposed techniques, consider the manifoldly ambiguous (but identifiable) scenario [7]

$$\boldsymbol{d}_1 = [0, 1.2, 3.4, 4.6]$$
$$\boldsymbol{w}_4 = [-0.8391, -0.4043, 0.0304, 0.4652]. \quad (55)$$

The problem is to estimate the true four sources $\boldsymbol{w}_4$ $(m = M)$ amongst the set of five ambiguous directions given by the co-array AGS $\boldsymbol{w}_{AGS} = [-0.8391, -0.4043, 0.0304, 0.4652, 0.9]$.

First, we investigate deterministic ME completion for this scenario at a SNR of 20 dB common to all four sources. The dotted line in Fig. 1 shows the ME spectrum of the augmented covariance matrix completed by the maximum-entropy criterion $H_{ME}$. For comparison, the dashed line shows $ME(H_{exact})$,

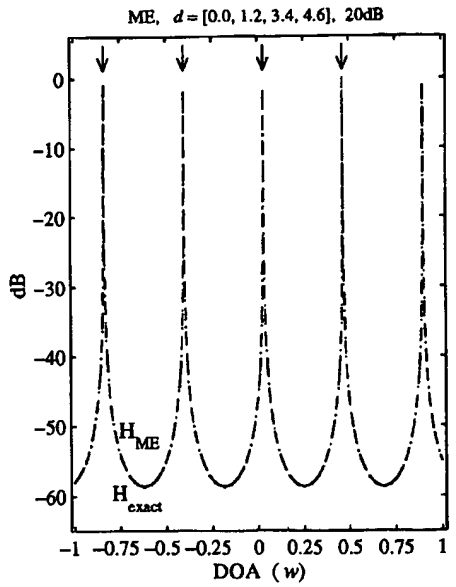


Fig. 1. ME spectra of the exact co-array covariance matrix $H_{exact}$ and the ME-completed matrix $H_{ME}$ for the AGS associated with the co-array of $\boldsymbol{d}$. Arrows indicate the four true DOA's.

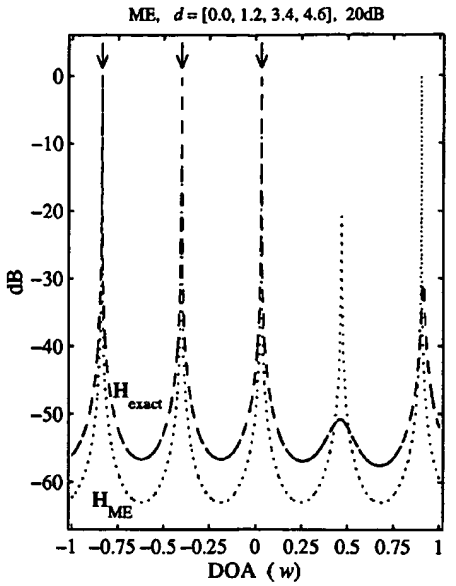


Fig. 2. Same as Fig. 1, except involving the first three DOA's in the AGS $\boldsymbol{w}_{AGS}$ (12).

which is the ME spectrum of the true covariance matrix, calculated using the co-array (our virtual array) $\boldsymbol{c}_1$. In this case, the ME-completed and the true ME spectra are essentially identical. Both spectra exhibit five strong peaks in the expected directions $\boldsymbol{w}_{AGS}$. The corresponding MUSIC pseudo-spectra (which is not shown) for $H_{exact}$ and $H_{ME}$ (and, indeed, the minimum-deflective completion $H_{MD}$) are all practically identical. The simple conclusion is that for this scenario, ME completion of the two missing lags produces results consistent with the DOA estimation problem.

To emphasize the point that ME completion is an *ad hoc* criterion, not necessarily consistent, and prone to "self-induced" ambiguity, we next consider the same scenario but with three DOA's:

$$\begin{aligned} \boldsymbol{d}_1 &= [0, 1.2, 3.4, 4.6] \\ \boldsymbol{w}_3 &= [-0.8391, -0.4043, 0.0304]. \end{aligned} \tag{56}$$

Recall that the ambiguity rank of the AGS $\boldsymbol{w}_{AGS}$ is equal to three for $\boldsymbol{d}_1$ and four for $\boldsymbol{c}_1$, i.e., this scenario is manifoldly ambiguous for the array *but not for the co-array*. Nevertheless, $ME(H_{ME})$ (as shown in dotted line in Fig. 2) once again exhibits all five peaks, unlike the ME spectrum of the true covariance matrix $ME(H_{exact})$ (dashed line). Meanwhile, the MUSIC pseudo-spectrum of $H_{ME}$ assuming $m = 3$ sources shows four strong peaks (which is not shown), unlike the three true DOA's indicated by $MUSIC(H_{exact})$. Moreover, $MUSIC(H_{ME})$, assuming four sources, presents all five peaks in the directions $\boldsymbol{w}_{AGS}$, similarly to $MUSIC(H_{ME})$ in the previous four-source scenario.

Thus, maximization of the determinant of the partially specified covariance matrix has the effect of changing this potentially co-array-unambiguous three-source scenario into an ambiguous four-source scenario, with the true directions being a subset of some new ambiguous DOA set.

**Ambiguity Resolution with Local Refinement (ARLR)**

Step 1: Given the ME- or MD-completed DAA-augmented covariance matrix $\hat{H}(17)$ obtained from the DDC matrix $\hat{R}(8)$, calculate the initial set of $\ell \geq m$ DOA estimates $\tilde{\boldsymbol{\theta}}_*$ by applying MUSIC to the $L$-variate matrix $\hat{H}$ and selecting all local maxima from the pseudo-spectrum. (If $\ell = m$, then there is no ambiguity: stop.)

Step 2: Solve the LP problem (51)–(54) to find the best-fit source power estimates $\hat{\tilde{\boldsymbol{p}}}_*$.

Step 3: Select the $m$ greatest elements of $\hat{\tilde{\boldsymbol{p}}}_*$ and treat the corresponding $m$ elements of $\hat{\tilde{\boldsymbol{\theta}}}_*$ as the initial set of unambiguous DOA estimates $\hat{\boldsymbol{\theta}}^{(0)}$.

Step 4: Calculate the set of refined unambiguous source powers $\hat{\boldsymbol{p}}^{(0)}$ by solving the LP problem (51)–(54) with the $m$ unambiguous DOA's $\hat{\boldsymbol{\theta}}^{(0)}$ substituted for the $\ell$ ambiguous DOA's $\tilde{\boldsymbol{\theta}}_*$.

Step 5: Apply the local ML search in the neighborhood of $(\hat{\boldsymbol{\theta}}^{(0)}, \hat{\boldsymbol{p}}^{(0)})$ to obtain $\hat{\boldsymbol{\theta}}^{(1)}$, as described for example in [11] (therein referred to as Step 4 of the ATML algorithm).

TABLE I
DOA AND POWER ESTIMATES OBTAINED VIA ME AND MD COMPLETION FOR EXACT COVARIANCE LAGS FOR THE FIG. 1 SCENARIO

| $\bar{w}_*$ | $\hat{w}_*^{MD}$ | $\hat{w}_*^{ME}$ | $\bar{p}_*$ | $\hat{p}_*^{MD}$ | $\hat{p}_*^{ME}$ |
|---|---|---|---|---|---|
| −0.8391 | −0.8348 | −0.8392 | 100.0000 | 74.2378 | 100.0004 |
| −0.4043 | −0.4096 | −0.4044 | 100.0000 | 96.6244 | 100.0101 |
| 0.0304 | 0.0356 | 0.0304 | 100.0000 | 100.0437 | 99.9921 |
| 0.4652 | 0.4608 | 0.4652 | 100.0000 | 103.1554 | 99.9974 |
| 0.9000 | 0.9044 | 0.9000 | 0.0000 | 25.9388 | $1.0\times10^{-10}$ |

Interestingly, in this four-source experiment, both ME and MD completions retain the true eigenspectrum quite accurately. In contrast, ME completion of $H$ in the three-source scenario results in a very significantly increased fourth eigenvalue (as a consequence of determinant-maximizing) and has allowed appreciable energy to leak into the noise subspace, thus creating a "self-induced" spurious extra source. Even MD completion displays a similar phenomenon, although not to the same extent. This proves our assertion that ME (and MD) completion is not always consistent with DOA estimation, and both should be regarded as *ad hoc* criteria.

Note that the three-source scenario $\boldsymbol{w}_3$ is identifiable with respect to $\boldsymbol{d}_1$; thus, all spurious directions can be easily removed by the "diagonal-fitting" method; more details on manifold ambiguity resolution in the conventional case can be found in [9].

Now, let us consider the accuracy of DOA estimation by our techniques. Table I presents the DOA and power estimates obtained by ME and MD completion using the true (deterministic) covariance lags and the diagonal-fit method for the above four-source scenario. In this particular case, ME completion yields almost ideal results, whereas MD completion is less accurate. However, the worst DOA error under the MD scheme (0.0052) is comparatively small since it corresponds to the CRB for almost 500 snapshots. Note that the inferior MD-completed DOA estimates have resulted in a considerable redistribution of power from the first (true) DOA to the fifth (false) DOA.

In order to demonstrate that the relative merits of ME and MD completion are scenario-dependent, we next consider the arbitrarily chosen unambiguous four-source scenario

$$\boldsymbol{d}_1 = [0, 1.2, 3.4, 4.6], \quad \boldsymbol{w}_{4a} = [-0.8, -0.3, 0.1, 0.4]. \quad (57)$$

Fig. 3 illustrates the MUSIC pseudo-spectrum of $H_{exact}$ (dashed line), $H_{ME}$ (dotted line), and $H_{MD}$ (dot-dashed line). Both completions exhibit a strong spurious peak near the direction $w = 0.9564$, where the true spectrum has an extremely small local maximum. This again shows that completion (especially ME completion) can self-induce ambiguity where none actually exists; because of this phenomenon, ambiguity resolution is a necessary part of the DOA estimation procedure. The existence of a scenario-dependent bias leaves room for an unconventional asymptotic accuracy behavior.

The second half of our simulation results deals with the stochastic case, where the statistical performance of our techniques can be established. Tables II and III summarize the results of stochastic experiments for the co-array-manifoldly ambiguous $(\boldsymbol{d}_1, \boldsymbol{w}_4)$ scenario and the unambiguous $(\boldsymbol{d}_1, \boldsymbol{w}_{4a})$ scenario,

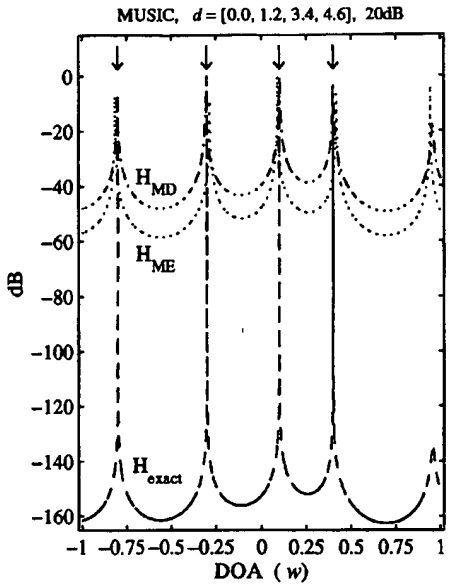


Fig. 3. MUSIC pseudo-spectra of $H_{exact}$, $H_{ME}$, and $H_{MD}$ for the unambiguous scenario $\boldsymbol{w}_{4a} = [-0.8, -0.3, 0.1, 0.4]$.

TABLE II
RESULTS OF STOCHASTIC SIMULATIONS FOR THE Fig. 1 SCENARIO, EACH WITH 1000 MONTE-CARLO TRIALS AND $N$ SNAPSHOTS

| | $N = 50$ | | $N = 200$ | | $N = 1000$ | |
|---|---|---|---|---|---|---|
| | $H_{MD}$ | $H_{ME}$ | $H_{MD}$ | $H_{ME}$ | $H_{MD}$ | $H_{ME}$ |
| Prob of correct identification | 0.520 | 0.754 | 0.502 | 0.887 | 0.493 | 0.997 |
| Unrefined bias | 0.0182 | 0.0017 | 0.0126 | 0.0007 | 0.0097 | 0.0003 |
| Unrefined standard dev | 0.0116 | 0.0011 | 0.0065 | 0.0003 | 0.0032 | 0.0001 |
| Refined bias | 0.0086 | | 0.0071 | | 0.0028 | |
| Refined standard dev | 0.0143 | | 0.0055 | | 0.0021 | |
| Cramér–Rao bound | 0.0157 | | 0.0078 | | 0.0035 | |

TABLE III
RESULTS OF STOCHASTIC SIMULATIONS FOR THE Fig. 3 SCENARIO, EACH WITH 1000 MONTE-CARLO TRIALS AND $N$ SNAPSHOTS

| | $N = 50$ | | $N = 200$ | | $N = 1000$ | |
|---|---|---|---|---|---|---|
| | $H_{MD}$ | $H_{ME}$ | $H_{MD}$ | $H_{ME}$ | $H_{MD}$ | $H_{ME}$ |
| Prob of correct identification | 0.909 | 0.934 | 0.994 | 0.999 | 1.000 | 1.000 |
| Unrefined bias | 0.0173 | 0.0260 | 0.0103 | 0.0220 | 0.0063 | 0.0200 |
| Unrefined standard dev | 0.0093 | 0.0063 | 0.0052 | 0.0036 | 0.0032 | 0.0019 |
| Refined bias | 0.0080 | | 0.0035 | | 0.0015 | |
| Refined standard dev | 0.0070 | | 0.0022 | | 0.0006 | |
| Cramér–Rao bound | 0.0055 | | 0.0027 | | 0.0012 | |

respectively. Each experiment consisted of 1000 Monte Carlo trials. Three different sample sizes ($N = 50, 200,$ and 1000) were simulated, each for ME and MD completion. The tables give the sample probability of correct identification (i.e., ambiguity resolution), the bias and standard deviation for the sample of worst DOA estimate in each trial, the same measures for the worst DOA estimate after ML refinement, and, finally, the CRB.

In the case of Table II, we see that (unrefined) DOA estimation accuracy provided by ME completion is very much better

than that given by MD completion, but more importantly, it is significantly better than the corresponding CRB. Moreover, local ML refinement merely degrades the ME initialization accuracy to a level comparable with the CRB. For the unambiguous scenario of Table III, we find that this remarkable phenomenon does not occur; instead, ME completion generates DOA estimates that are significantly biased and worse than the CRB, as we would have expected. We are forced to conclude that ME completion for the Table II scenario yields DOA estimates that are known in statistical estimation theory as *super-efficient* [18].

Let us now turn our attention to the probabilities of correct initialization (ambiguity resolution) for these two scenarios. In the first case, despite the extremely accurate super-efficient ME estimates, the probability of correctly resolving the ambiguity is merely quite good, increasing to 99.7% for $N = 1000$ snapshots. This reveals that the diagonal-fitting method can be very sensitive to DOA estimation errors. For this reason, MD completion (that is significantly less accurate than ME completion in this case) has no chance to resolve ambiguity; for all our experiments, the probability of correct identification was essentially equal to one half, and the power estimates for the first (true) and fifth (spurious) source averaged around 50 each. Only when the sample size was increased to $N = 10^4$ did this probability increase to 67.5%, whereas only for $N = 5 \times 10^5$ were all 1000 trials correctly identified. For the unambiguous Table III scenario, both completion techniques demonstrate a very high probability of correct identification for a very modest sample volume, despite significant DOA initialization inaccuracies.

Thus, we may conclude that the NLA $\boldsymbol{d}_1$ and AGS $\boldsymbol{w}_{AGS}$ introduced in [7] has two additional remarkable properties. First, DOA estimates produced by ME completion are super-efficient. Second, due to the above example, we may introduce the concept of *unstable identifiability* since neither local nonidentifiability (rank deficiency of the Fisher information matrix) nor pointwise nonidentifiability apply in this case. Here, we have demonstrated the ability to unmistakably resolve this ambiguity for the exact covariance lags and DOA's; however, in a small neighborhood of these values, the solution of the LP problem bifurcates, and therefore, the problem is identifiable only for an extremely large sample size (which is not always possible in practice). This phenomenon is well-known in the field of perturbation analysis in mathematical programming [26].

Thus, any identifiable scenario that is unstable in some small neighborhood of the true parameters $(\boldsymbol{r}, \tilde{\boldsymbol{\theta}}_*)$ may be called unstably identifiable since for practical applications with a finite sample size $N$, this property actually means that the scenario is nonidentifiable unless $N$ is several orders of magnitude larger than in stably identifiable scenarios.

It might be interesting also to comment on the feasibility statistics of p.d. completion for the incomplete augmented sample covariance matrix. For the Table III scenario, for example, the feasibility condition $H(\boldsymbol{z}) > 0$ did not hold in about 24% of our 1000 trials for $N = 50$ snapshots, and hence, the modification of the specified covariance lags as described in Section III-C was applied. For $N = 200$, this probability decreased to 11%, whereas for $N = 1000$, a single infeasible trial was found. For the more sensitive Table II scenario, the probabilities were not surprisingly higher: approximately 46% for $N = 50, 200$, and 1000, dropping to 26% only for $N = 10^4$. Interestingly, these probabilities are quite close to those of incorrect identification produced by MD completion in this case.

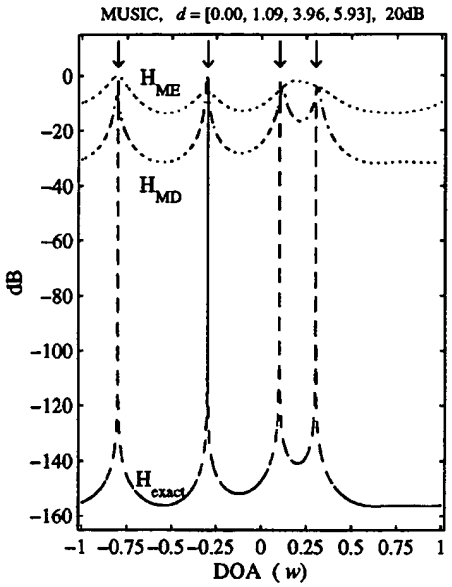


Fig. 4. MUSIC pseudo-spectra of $H_{exact}$, $H_{ME}$, and $H_{MD}$ for the unambiguous scenario $\boldsymbol{w}_{4b} = [-0.8, -0.3, 0.1, 0.3]$ and "GIMP-identifiable" array $\boldsymbol{d}_2$.

Our final example deals with the quasi-fully augmentable and GIMP-identifiable array

$$\boldsymbol{d}_2 = [0, 1.09, 3.96, 5.93] \tag{58}$$

that has the potential to unambiguously identify up to six uncorrelated sources. We will first demonstrate that MD completion can be an improvement on ME completion by considering the $m = 4$ scenario

$$\boldsymbol{w}_{4b} = [-0.8, -0.3, 0.1, 0.3]. \tag{59}$$

Of course, $M = 4$ is not sufficiently large to expect extreme consequences of the augmented covariance matrix incompleteness; however, by beginning matrix completion with the true covariance matrix $R_{exact}$, the MUSIC pseudo-spectrum of $H_{MD}$ (dot-dashed line in Fig. 4) clearly demonstrates an accurate and consistent identification that is very close to the ideal pseudo-spectrum $MUSIC(H_{exact})$ (dashed line), whereas $MUSIC(H_{ME})$ (dotted line) has only three peaks. Obviously, the initialization approach we have proposed cannot work properly via ME completion for this scenario. This emphasizes that neither ME nor MD completion is an ideal technique for DOA estimation and that further work into completion philosophies is necessary.

Finally, we consider the equispaced six-source superior scenario

$$\begin{aligned} \boldsymbol{d}_2 &= [0, 1.09, 3.96, 5.93] \\ \boldsymbol{w}_6 &= [-0.80, -0.47, -0.14, 0.19, 0.52, 0.85]. \end{aligned} \tag{60}$$

The first block of data in Table IV presents the results of stochastic simulations, each involving 1000 Monte Carlo trials for 20 dB SNR and $N = 200$ snapshots. Here, we are only in-

TABLE IV
RESULTS OF STOCHASTIC SIMULATIONS FOR INITIALIZATION IN THE UNAMBIGUOUS SIX-SOURCE SCENARIO AND A "GIMP-IDENTIFIABLE" ARRAY FOR VARIOUS INTERSOURCE CORRELATION COEFFICIENTS $\alpha$; 1000 MONTE-CARLO TRIALS AND 200 SNAPSHOTS. CRB FOR $\alpha = 0$ IS EQUAL TO 0.0032

| | $\alpha = 0$ | | $\alpha = 0.1$ | | $\alpha = 0.5$ | | $\alpha = 1.0$ | |
|---|---|---|---|---|---|---|---|---|
| | $H_{MD}$ | $H_{ME}$ | $H_{MD}$ | $H_{ME}$ | $H_{MD}$ | $H_{ME}$ | $H_{MD}$ | $H_{ME}$ |
| Unrefined bias | 0.0107 | 0.0106 | 0.0108 | 0.0112 | 0.0126 | 0.0153 | 0.0155 | 0.0172 |
| Unrefined standard dev | 0.0041 | 0.0016 | 0.0038 | 0.0015 | 0.0015 | 0.0005 | 0.0006 | 0.0003 |

terested in comparing initialization accuracy between ME and MD completions since the asymptotic efficiency of the local ML refinement procedure has already been demonstrated. As before, the bias and standard deviation for the worst DOA estimate is given. This scenario with well-separated sources is almost equally well initialized by either completion.

The final important issue that needs to be addressed is related to our basic assumption that there is no intersource correlation, i.e., that the matrix $P$ in (4) and (7) is purely diagonal. In any practical application, there might be some residual nonzero intersource correlation that should be tolerated by our approach without a significant degradation in performance. In order to investigate this issue, we have repeated the stochastic experiments for the last six-source scenario, modifying the intersource correlation matrix in the following way:

$$P = 10^{SNR/10}(I_m + \alpha \mathbf{1}_m) \tag{61}$$

where $\mathbf{1}_m$ is the $m$-variate unit matrix for $\alpha = 0.1, 0.5, 1.0$. This model represents $m$ independent sources and their fully correlated component. We can see from Table IV that the initialization accuracy does not dramatically degrade as the intersource correlation increases.

We deliberately have not performed local DOA refinement for both uncorrelated and correlated trials (for different reasons). It is important to emphasize that augmentation relies on the uncorrelated-source model, whereas the refinement procedure could, in principle, incorporate any specific model for the intersource correlation matrix $P$. Since augmentation is here used for initialization only, it would be straightforward to introduce modifications incorporating such a model.

Computationally, both ME- and MD-completion techniques are very efficient, especially compared with the computationally intensive one-dimensional (1-D) local ML search.

## VII. SUMMARY AND CONCLUSIONS

This paper demonstrates that the DOA estimation problem for noninteger nonuniform linear arrays may be successfully solved for a *superior* number of *identifiable* uncorrelated Gaussian sources. We have formulated necessary and sufficient conditions for both *local* and *pointwise* nonidentifiability. The former means that the Fisher information matrix is rank deficient, whereas the latter means that the $m$-source covariance matrix is identical to some similar mixture of $m$ independent sources with at least one different DOA. Pointwise nonidentifiability is defined by the algebraic properties of the particular array geometry $\boldsymbol{d}$ and DOA scenario $\boldsymbol{w}$. Since one of the necessary conditions for this type of nonidentifiability is manifold ambiguity in the co-array, the Proukakis–Manikas technique [7], [8] for computing ambiguity generator sets (AGS's) is used to list potentially nonidentifiable scenarios for any given array in order to test each of them against the pointwise nonidentifiability condition.

Both of these types of nonidentifiability are *strict* in the sense that they occur for true values of DOA's and covariance lags. By an example, we have also established the existence of a different type of *unstable identifiability*, which is important when considering practical applications. This occurs in scenarios that are theoretically identifiable, i.e. for true values, and where our proposed method can perfectly resolve ambiguity (again for true DOA's and covariance lags) but where for very small estimation errors, the LP solution bifurcates, meaning that the scenario is identifiable only for an extremely large sample size (which is not always possible in practice). It seems to be more than coincidental that the same example of unstable identifiability also demonstrates *super-efficient* DOA estimates with one of the matrix completion methods we have discussed. Nevertheless, even this remarkable DOA estimation accuracy, which is far better than predicted by Cramér-Rao bound analysis, does not result in near-perfect ambiguity resolution due to the great sensitivity of the problem.

These phenomena have been demonstrated using a rather unusual array (noninteger but still highly redundant), introduced in [7] to illustrate high-order ambiguity. From this viewpoint, *GIMP-identifiable* arrays are introduced here as a preferred geometry; this class does not satisfy the co-array manifold ambiguity condition, and therefore, such arrays are *globally* identifiable (for independent Gaussian sources), modulo the unproven completeness of the AGS-generating technique. For *quasi-fully augmentable* (noninteger) geometries that can be treated as slightly perturbed versions of some corresponding fully augmentable (integer) array, we conjecture (for independent Gaussian sources) that for sufficiently small perturbations, such geometries are also strictly globally identifiable (regardless of the AGS-generating completeness).

Our approach to DOA estimation for noninteger linear arrays with an equal or greater number of uncorrelated sources than sensors (the *superior* case) essentially consists of three steps. In the first initialization stage, we associate our problem with some completion of the partially specified Hermitian covariance matrix corresponding to a particular *virtual* array. We have proposed that the co-array is the logical choice for this virtual array. The specified elements of the Hermitian matrix are estimated using the direct augmentation approach (DAA) applied to the standard direct data covariance (DDC) matrix. Two *ad hoc* completion criteria have been discussed: maximum-entropy (ME) and minimum-deflective (MD). For ME completion, a unique optimum

solution is guaranteed for any feasible initial set of specified covariance lags. A similar uniqueness is guaranteed for MD completion, which was devised for slightly perturbed integer array (quasi-integer) geometries but may be applied in all cases.

The feasibility condition, which is evidently satisfied by the existence of the true values of the specified covariance lags, generally does not hold in the practical case of sample covariance lags. We used computationally efficient interior-point convex programming routines to modify these stochastic covariance lags (if necessary), resulting in the global extremum of this sample covariance matrix completion problem.

These two completion methods provide a reasonable initialization accuracy in many cases; nevertheless, it is important to emphasize that both these *ad hoc* criteria are not always consistent with the maximum-likelihood (ML) principle and may be inappropriate for DOA estimation in some cases. For the ME criterion, this is well known since the famous ME (Burg) spectrum can be poorly consistent with DOA estimation. We have demonstrated that ME completion has, apart from a possible DOA bias, the potential to increase the signal subspace, i.e., to create a *self-induced* ambiguity or, on the contrary, to increase the "white noise level" (minimum eigenvalue) to submerge poorly separated sources in the new "noise level." Both these phenomena are direct consequences of its determinant-maximizing nature.

The nonoptimality of both these initializing completion methods has made it necessary to improve the accuracy of the DOA estimates by introducing two subsequent refinement steps. The purpose of the first refinement procedure is to resolve possible co-array manifold ambiguity and/or self-induced ambiguity. For all (stably) identifiable scenarios, the proposed linear programming routine is able to resolve these ambiguities with a reasonably high probability.

The second refinement step is applied to the set of now unambiguous DOA's and implements a local ML search in the neighborhood of the initial DOA estimates. This is necessary to remove a possible bias introduced by completion and to ensure that the final accuracy is close to the CRB. The latter is important because the DAA is known to be far from asymptotically optimal [11]. Even so, the biased nature of the DOA estimates produced by ME completion has left room for super-efficient DOA initialization in one particular presented scenario. In less exotic examples and, specifically, for GIMP-identifiable arrays, our approach demonstrates almost CRB-optimal final accuracy. Finally, we have also seen that the augmentation technique, which relies on the uncorrelated sources model, is quite robust with respect to a finite amount of intersource correlation.

## REFERENCES


[1] J.-J. Fuchs, "Extension of the Pisarenko method to sparse linear arrays," in *Proc. Int. Conf. Acoust., Speech Signal Process.*, Detroit, MI, 1995, pp. 2100–2103.

[2] K. Sharman, "Maximum likelihood parameter estimation by simulated annealing," in *Proc. Int. Conf. Acoust., Speech Signal Process.*, New York, 1988, pp. 2741–2744.

[3] J.-J. Fuchs, "The rectangular Pisarenko method," in *Proc. Int. Conf. Acoust., Speech Signal Process.*, Atlanta, GA, 1996, pp. 2495–2498.

[4] Y. I. Abramovich, N. K. Spencer, and A. Y. Gorokhov, "Generalised augmentation approach for arbitrary linear antenna arrays," in *Proc. Int. Conf. Acoust., Speech Signal Process.*, vol. 5, Munich, Germany, 1997, pp. 3757–3760.

[5] J.-F. Cardoso, "Source separation using higher order moments," in *Proc. Int. Conf. Acoust., Speech Signal Process.*, 1989, pp. 2109–2112.

[6] Y. I. Abramovich, N. K. Spencer, and A. Y. Gorokhov, "Positive-definite Toeplitz completion in DOA estimation for nonuniform linear antenna arrays—Part II: Partially-augmentable arrays," *IEEE Trans. Signal Processing*, vol. 47, pp. 1502–1521, June 1999.

[7] C. Proukakis and A. Manikas, "Study of ambiguities of linear arrays," in *Proc. Int. Conf. Acoust., Speech Signal Process.*, vol. 4, Adelaide, Australia, 1994, pp. 549–552.

[8] A. Manikas and C. Proukakis, "Modeling and estimation of ambiguities in linear arrays," *IEEE Trans. Signal Processing*, vol. 46, pp. 2166–2179, Aug. 1998.

[9] Y. I. Abramovich, N. K. Spencer, and A. Y. Gorokhov, "Resolving manifold ambiguities in direction-of-arrival estimation for nonuniform linear antenna arrays," *IEEE Trans. Signal Processing*, vol. 47, pp. 2629–2643, Oct. 1999.

[10] P. Stoica and A. Nehorai, "Performance study of conditional and unconditional direction-of-arrival estimation," *IEEE Trans. Acoust., Speech Signal Processing*, vol. 38, pp. 1783–1795, Oct. 1990.

[11] Y. I. Abramovich, D. A. Gray, A. Y. Gorokhov, and N. K. Spencer, "Positive-definite Toeplitz completion in DOA estimation for nonuniform linear antenna arrays—Part I: Fully-augmentable arrays," *IEEE Trans. Signal Processing*, vol. 46, pp. 2458–2471, Sept. 1998.

[12] S. Boyd, L. El Ghaoui, E. Feron, and V. Balakrishnan, *Linear Matrix Inequalities in System and Control Theory*. Philadelphia, PA: SIAM, 1994, vol. 15.

[13] M. E. Lundquist and C. R. Johnson, "Linearly constrained positive definite completions," *Linear Algebra Appl.*, vol. 150, pp. 195–208, 1991.

[14] R. Grone, C. R. Johnson, E. Marques de Sá, and H. Wolkowicz, "Positive definite completions of partial Hermitian matrices," *Linear Algebra Appl.*, vol. 58, pp. 109–124, 1984.

[15] S. Haykin, *Adaptive Filter Theory*, 3rd ed. Englewood Cliffs, NJ: Prentice-Hall, 1996.

[16] Y. Nesterov and A. Nemirovskii, *Interior-Point Polynomial Algorithms in Convex Programming*. Philadelphia, PA: SIAM, 1994, vol. 13.

[17] A. T. Moffet, "Minimum-redundancy linear arrays," *IEEE Trans. Antennas Propagat.*, vol. AP–16, pp. 172–175, Feb. 1968.

[18] B. Porat, *Digital Processing of Random Signals*, 5th ed. Englewood Cliffs, NJ: Prentice-Hall, 1994.

[19] S. Kullback, *Information Theory and Statistics*, P. Smith, Ed. London, U.K., 1978.

[20] M. J. D. Rendas and J. M. F. Moura, "Ambiguity in radar and sonar," *IEEE Trans. Signal Processing*, vol. 46, pp. 294–305, Feb. 1998.

[21] Y. I. Abramovich, D. A. Gray, N. K. Spencer, and A. Y. Gorokhov, "Ambiguities in direction-of-arrival estimation for nonuniform linear antenna arrays," in *Proc. ISSPA*, Gold Coast, Australia, 1996, pp. 631–634.

[22] Y. I. Abramovich, N. K. Spencer, and A. Y. Gorokhov, "Identifiability and manifold ambiguity in DOA estimation for nonuniform linear antenna arrays," in *Proc. Int. Conf. Acoust., Speech, Signal Process.*, vol. 5, Phoenix, AZ, 1999, pp. 2845–2848.

[23] H. A. d'Assumpçao, "Some new signal processors for arrays of sensors," *IEEE Trans. Inform. Theory*, vol. IT-26, pp. 441–453, July 1980.

[24] J.-J. Fuchs, "Extension of the Pisarenko method to sparse linear arrays," *IEEE Trans. Signal Processing*, vol. 45, pp. 2413–2421, Oct. 1997.

[25] Y. I. Abramovich and M. B. Sverdlik, "Certain problems in the optimization of radiation patterns of antenna arrays according to the minimax criterion," *Radio Eng. Electron. Phys.*, vol. 19, no. 10, pp. 119–121, 1974.

[26] A. A. Pervozvanskii and V. G. Gaitsgori, *Theory of Suboptimal Decisions*. Dordrecht, The Netherlands: Kluwer, 1988.



**Yuri I. Abramovich** (M'96) received the Dipl.Eng. (Hons.) degree in radio electronics in 1967 and the Cand.Sci. degree (Ph.D. equivalent) in theoretical radio techniques in 1971, both from the Odessa Polytechnic University, Odessa, Ukraine, and in 1981, he received the D.Sc. degree in radar and navigation from the Leningrad Institute for Avionics, Leningrad, Russia.

From 1968 to 1994, he was with the Odessa State Polytechnic University, Odessa, Ukraine, as a Research Fellow, Professor, and ultimately as Vice-Chancellor of Science and Research. Since 1994, he has been at the Cooperative Research Centre for Sensor Signal and Information Processing (CSSIP), Adelaide, Australia. His research interests are in signal processing (particularly spatio-temporal adaptive processing, beamforming, signal detection and estimation), its application to radar (particularly over-the-horizon radar), electronic warfare, and communication.

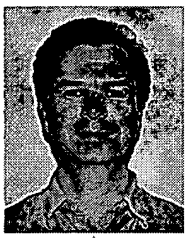

**Nicholas K. Spencer** received the B.Sc. (Hons.) degree in applied mathematics in 1985 and the M.Sc. degree in computational mathematics in 1992, both from the Australian National University, Canberra.

His has been with the Australian Department of Defence, the Flinders University of South Australia, the University of Adelaide, and the Australian Centre for Remote Sensing in the areas of computational and mathematical sciences. He is currently a Research Fellow at the Cooperative Research Centre for Sensor Signal and Information Processing (CSSIP), Adelaide, Australia. His research interests include array signal processing, parallel and supercomputing, numerical solution of partial differential equations, theoretical astrophysics, and cellular automata.

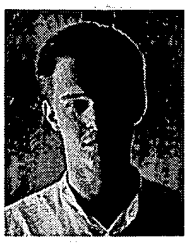

**Alexei Y. Gorokhov** (M'96) received the Dipl.Eng. (Hons.) degree in radio electronics in 1993 from the Odessa State Polytechnic University, Odessa, Ukraine. From 1993 to 1994, he was with the Scientific Research Department of the same university. From 1994 to 1997, he was pursuing the Ph.D. degree in signal processing at Télécom Paris, Paris, France.

He is currently a Research Fellow with the Centre Nationale de la Recherche Scientifique (CNRS), Laboratoire des Signaux et Systèmes (L2S), Paris. His research interests are in adaptive signal processing and blind signal separation and equalization in the application areas of radar, electronic warfare, and communications.